

Detection and estimation of vertex-wise latent position shifts across networks

Runbing Zheng

Department of Applied Mathematics and Statistics, Johns Hopkins University

February 5, 2025

Abstract

Pairwise network comparison is essential for various applications, including neuroscience, disease research, and dynamic network analysis. While existing literature primarily focuses on comparing entire network structures, we address a vertex-wise comparison problem where two random networks share the same set of vertices but allow for structural variations in some vertices, enabling a more detailed and flexible analysis of network differences. In our framework, some vertices retain their latent positions between networks, while others undergo shifts. To identify the shifted and unshifted vertices and estimate their latent position shifts, we propose a method that first derives vertex embeddings in a low-rank Euclidean space for each network, then aligns these estimated vertex latent positions into a common space to resolve potential non-identifiability, and finally tests whether each vertex is shifted or not and estimates the vertex shifts. Our theoretical results establish the test statistic for the algorithms, guide parameter selection, and provide performance guarantees. Simulation studies and real data applications, including a case-control study in disease research and dynamic network analysis, demonstrate that the proposed algorithms are both computationally efficient and effective in extracting meaningful insights from network comparisons.

Keywords: pairwise network comparison, random dot product graphs, latent position shifts, $2 \rightarrow \infty$ norm, normal approximations

1 Introduction

Pairwise network comparison is of both theoretical and practical importance, with applications across various fields including neuroscience [Tang et al., 2017a, Van Wijk et al., 2010, Zalesky et al., 2010], case-control studies in disease research [Segerstolpe et al., 2016], and dynamic network analysis [Liu et al., 2018]. For instance, comparing the brain networks of individuals in case and control groups for a particular disease can help identify neurological characteristics associated with the disease and provide insights into the underlying mechanisms. For dynamic network analysis and its related challenges, such as understanding or visualizing its overall evolution patterns and detecting change points, we frequently need to study the similarity between two networks constructed using disjoint time intervals. For example, when analyzing the trading network of a specific product among different countries over several years, comparing the trading networks for each pair of years enables the study of the product’s trading network evolution over time.

Existing literature on pairwise network comparison primarily focuses on testing whether the *entire* underlying network structures of two independent networks on the same set of vertices are equivalent. Ghoshdastidar et al. [2017] consider two networks generated from two distributions, and provide a framework for formulating the two-sample hypothesis testing problem to determine whether the generating distributions of two networks are sufficiently similar with minimal structural assumptions. Ghoshdastidar et al. [2020] study inhomogeneous random network models with population Bernoulli probability matrices $\mathbf{P}^{(1)}$ and $\mathbf{P}^{(2)}$, where multiple independent and identically distributed networks are available for each $\mathbf{P}^{(i)}$, and analyze the minimax separation rate ρ^* for the threshold ρ in testing $\mathbf{P}^{(1)} = \mathbf{P}^{(2)}$ against $d(\mathbf{P}^{(1)}, \mathbf{P}^{(2)}) > \rho$ for some common choices of the distance function $d(\cdot, \cdot)$. Tang et al. [2017a,b] consider the problem of comparing two random dot product graphs (RDPGs) [Athreya et al., 2018, Young and Scheinerman, 2007] with probability matrices $\mathbf{P}^{(1)} = \mathbf{X}^{(1)}\mathbf{X}^{(1)\top}$ and $\mathbf{P}^{(2)} = \mathbf{X}^{(2)}\mathbf{X}^{(2)\top}$, where the k th row of $\mathbf{X}^{(i)}$, $\mathbf{x}_k^{(i)}$, represents

the latent position of vertex k in network i . Tang et al. [2017b] suppose that the latent positions of all vertices in each network are i.i.d. following distributions $F^{(1)}$ and $F^{(2)}$, respectively, i.e., $\{\mathbf{x}_k^{(1)}\}_k \stackrel{\text{i.i.d.}}{\sim} F^{(1)}$ and $\{\mathbf{x}_k^{(2)}\}_k \stackrel{\text{i.i.d.}}{\sim} F^{(2)}$, and propose a hypothesis test to determine whether $F^{(1)} = F^{(2)} \circ U$ for some unitary operator U , which is equivalent to testing whether the two RDPGs are identically distributed. Tang et al. [2017a] study a more general problem by relaxing the i.i.d. assumption for vertices and testing whether the latent position matrices $\mathbf{X}^{(1)}$ and $\mathbf{X}^{(2)}$ are the same up to an orthogonal transformation, i.e., $\mathbf{X}^{(1)} = \mathbf{X}^{(2)}\mathbf{W}^{(1,2)}$ for some orthogonal $\mathbf{W}^{(1,2)}$, which is equivalent to testing whether the probability matrices $\mathbf{P}^{(1)}$ and $\mathbf{P}^{(2)}$ are identical. Li and Li [2018] consider two networks generated from weighted stochastic block models and propose a hypothesis test to assess whether the community assignments of all vertices in the two networks are the same. Jin et al. [2024] study networks generated from the degree-corrected mixed-membership model allowing degree heterogeneity and mixed memberships, and propose the interlacing balance measure to test whether the underlying Bernoulli probability matrices $\mathbf{P}^{(1)}$ and $\mathbf{P}^{(2)}$ of the two networks are the same.

Instead of comparing the *entire* underlying structures of two networks, in this paper we conduct a *vertex-wise* comparison between two random networks that share the same set of vertices while allowing for structural variations in some vertices. Specifically we consider two independent RDPGs on the same set of vertices, and suppose that some vertices remain latent positions while others experience latent position shifts. The subset of unshifted vertices, denoted as \mathcal{U} , retains the same latent positions between the two networks (up to an orthogonal transformation considering the orthogonal nonidentifiability in RDPGs), i.e., $\mathbf{X}_{\mathcal{U}}^{(1)} = \mathbf{X}_{\mathcal{U}}^{(2)}\mathbf{W}^{(1,2)}$ for some orthogonal $\mathbf{W}^{(1,2)}$. The remaining vertices in \mathcal{U}^c undergo shifts in their latent positions, given by $\mathbf{X}_{\mathcal{U}^c}^{(1)} = \mathbf{X}_{\mathcal{U}^c}^{(2)}\mathbf{W}^{(1,2)} + \mathbf{Y}_{\mathcal{U}^c}$ where the shift matrix $\mathbf{Y}_{\mathcal{U}^c}$ has no zero rows. Notice that the two networks preserve the pairwise connection probabilities within \mathcal{U} , i.e., $\mathbf{P}_{\mathcal{U},\mathcal{U}}^{(1)} = \mathbf{P}_{\mathcal{U},\mathcal{U}}^{(2)}$, and the probabilities outside this submatrix typically change.

Given the observed adjacency matrices of the pair of networks, we aim to (1) identify the unshifted and shifted vertices, i.e., determine \mathcal{U} , and (2) estimate the latent position shifts in $\mathbf{Y}_{\mathcal{U}^c}$. To the best of our knowledge, this model allowing for partial vertex-wise latent position shifts is novel.

A motivating example provides real-data evidence for the presence of both shifted and unshifted vertices in network comparisons. We compare the estimated vertex latent positions of two chocolate trading networks from the years 2010 and 2022 (with further details provided in Section 6.2). Figure 1 presents the 2-dimensional latent position estimates of 10 countries, where black stars represent the 5 countries with non-significant shifts, and colored stars represent the 5 countries exhibiting significant shifts. This real-world example naturally motivates our problem formulation. Another motivating example for our model

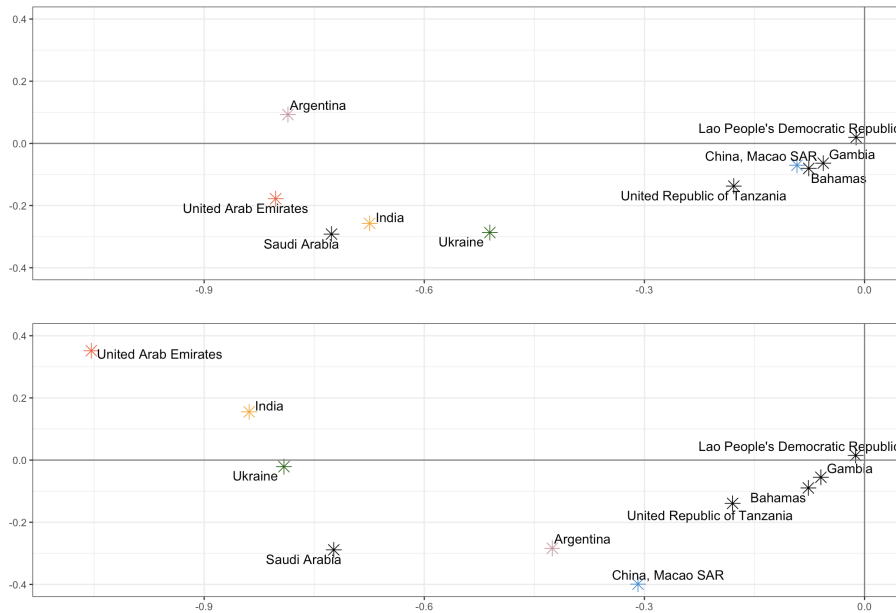


Figure 1: Estimated latent positions of 10 countries in the chocolate-trading networks in year 2010 (upper panel) and year 2022 (lower panel), with 5 countries (black) having non-significant latent position shifts and 5 countries (colored) having significant latent position shifts.

arises from stochastic block models (SBMs) [Holland et al., 1983] with block assignment switching. More specifically, we consider SBMs that share the same block probability matrix but allow some vertices to switch their block assignments between the two networks.

In this case identifying the vertices with shifted latent positions is equivalent to detecting those that have changed their block assignments (see Section 5.4 for details on the SBM setting and related experiments).

The vertex-wise comparison between networks can have significant practical implications in various real-world problems. For instance, in disease research if we only conduct an entire-network-level comparison between the brain networks of individuals in the case and control groups, we can merely determine whether the disease is generally associated with the overall brain network structure. But by performing a vertex-wise comparison, we can identify specific brain regions associated with the disease, which is crucial for more detailed analysis and understanding of its mechanisms. Another example is in trading networks. As shown in Figure 1, a vertex-wise comparison allows us to identify specific countries whose trading patterns have changed between the two years. Consequently, when considering a dynamic trading network over a sequence of years, we can analyze how a specific country’s trading pattern evolves over time. The vertex-wise comparison model thus provides a new perspective for studying the evolution of dynamic networks by tracking structural changes at the level of individual vertex shifts.

Based on existing entire-network comparison methods [Ghoshdastidar et al., 2017, 2020, Jin et al., 2024, Li and Li, 2018, Tang et al., 2017a,b], a natural idea to identifying the unshifted vertices would be to examine all possible subsets of vertices and apply an existing algorithm to test whether the corresponding subnetworks share the same underlying structure between the two networks. However, this approach incurs a computational cost of approximately 2^n times the complexity of the original algorithm, rendering it infeasible for large networks. Thus, there is a need to develop specialized and efficient algorithms tailored to the vertex-wise network comparison problem. We first consider a simple scenario where a (possibly very limited) subset of unshifted vertices, termed the seed set, is known, and propose a seed-based algorithm that aligns the estimated latent positions between the

two networks according to the seed set to identify the entire set of unshifted vertices \mathcal{U} and estimate the latent position shifts in $\mathbf{Y}_{\mathcal{U}^c}$. Building on the seed-based algorithm, we further develop a seed-free algorithm that does not rely on any prior knowledge of unshifted vertices, making it more practical for real-world applications. The key idea is to randomly generate some small subsets of vertices as candidate seed sets, apply the seed-based algorithm to each candidate, and ultimately select the candidate seed set that achieves the best alignment, i.e., yielding the largest number of unshifted vertices, as the most likely correct seed set.

Our theoretical results derive the test statistic used in the algorithms, guide the choice of parameters, and provide theoretical guarantees for the performance of the algorithms. In particular, we derive an error bound in the two-to-infinity norm for the estimated shift matrix, and using this error bound, we show that for each vertex, the estimated shift vector is approximately normally distributed around the true shift vector. Leveraging the normal approximation result, we construct a test statistic for each vertex, and show that the limiting distribution of this test statistic converges to a central χ^2 distribution under the null hypothesis of no shift and to a non-central χ^2 distribution under a local alternative hypothesis where a shift exists. The test statistic is used in our proposed algorithms to identify unshifted and shifted vertices. The error bound result also shows that the algorithms achieve consistent estimation even with only a minimal number of seed vertices, providing insights into parameter choice for the algorithms to achieve strong performance while maintaining computational efficiency.

The structure of our paper is as follows. In Section 2 we introduce the model for a pair of independent RDPGs with partially shifted vertices. In Section 3, we first propose the seed-based algorithm and then build upon it to develop the seed-free algorithm. We also analyze the computational complexity of the algorithms. Theoretical results for our algorithms are presented in Section 4. We have numerical simulations in Section 5, and

have real data experiments, including a brain network contrastive study and an analysis of the dynamic chocolate trading network, in Section 6. In Section 7, we integrate vertex-wise comparison with the mirror idea from Athreya et al. [2024] to analyze dynamic network evolution patterns, and we finally extend vertex-wise comparison from RDPGs to generalized RDPGs (GRDPGs) [Rubin-Delanchy et al., 2017, Young and Scheinerman, 2007], where the probability matrices take the more flexible form $\mathbf{P}^{(i)} = \mathbf{X}^{(i)} \mathbf{I}_{d_+, d_-} \mathbf{X}^{(i)\top}$ with diagonal matrix \mathbf{I}_{d_+, d_-} containing d_+ diagonal entries of $+1$ and d_- diagonal entries of -1 . Detailed proofs of stated results and additional experiment results are provided in the supplementary material.

1.1 Notations

We summarize some notations used in this paper. For any positive integer n , we denote by $[n]$ the set $\{1, 2, \dots, n\}$. For two non-negative sequences $\{a_n\}_{n \geq 1}$ and $\{b_n\}_{n \geq 1}$, we write $a_n \lesssim b_n$ (resp. $a_n \gtrsim b_n$) if there exists some constant $C > 0$ such that $a_n \leq Cb_n$ (resp. $a_n \geq Cb_n$) for all $n \geq 1$, and we write $a_n \asymp b_n$ if $a_n \lesssim b_n$ and $a_n \gtrsim b_n$. The notation $a_n \ll b_n$ (resp. $a_n \gg b_n$) means that there exists some sufficiently small (resp. large) constant $C > 0$ such that $a_n \leq Cb_n$ (resp. $a_n \geq Cb_n$). If a_n/b_n stays bounded away from $+\infty$, we write $a_n = O(b_n)$ and $b_n = \Omega(a_n)$, and we use the notation $a_n = \Theta(b_n)$ to indicate that $a_n = O(b_n)$ and $a_n = \Omega(b_n)$. If $a_n/b_n \rightarrow 0$, we write $a_n = o(b_n)$ and $b_n = \omega(a_n)$. We say a sequence of events \mathcal{A}_n holds with high probability if for any $c > 0$ there exists a finite constant n_0 depending only on c such that $\mathbb{P}(\mathcal{A}_n) \geq 1 - n^{-c}$ for all $n \geq n_0$. We write $a_n = O_p(b_n)$ (resp. $a_n = o_p(b_n)$) to denote that $a_n = O(b_n)$ (resp. $a_n = o(b_n)$) holds with high probability. We denote by \mathcal{O}_d the set of $d \times d$ orthogonal matrices. For any matrix $\mathbf{M} \in \mathbb{R}^{A \times B}$ and index sets $\mathcal{A} \subseteq [A]$, $\mathcal{B} \subseteq [B]$, we denote by $\mathbf{M}_{\mathcal{A}, \mathcal{B}} \in \mathbb{R}^{|\mathcal{A}| \times |\mathcal{B}|}$ the submatrix of \mathbf{M} formed from rows \mathcal{A} and columns \mathcal{B} , and we denote by $\mathbf{M}_{\mathcal{A}} \in \mathbb{R}^{|\mathcal{A}| \times B}$ the submatrix of \mathbf{M} consisting of the rows indexed by \mathcal{A} . Given a matrix \mathbf{M} , we denote its

spectral, Frobenius, and infinity norms by $\|\mathbf{M}\|$, $\|\mathbf{M}\|_F$, and $\|\mathbf{M}\|_\infty$, respectively. We also denote the maximum entry (in modulus) of \mathbf{M} by $\|\mathbf{M}\|_{\max}$ and the two-to-infinity norm of \mathbf{M} by

$$\|\mathbf{M}\|_{2 \rightarrow \infty} = \max_{\|\mathbf{x}\|=1} \|\mathbf{M}\mathbf{x}\|_\infty = \max_i \|\mathbf{m}_i\|,$$

where \mathbf{m}_i denotes the i th row of \mathbf{M} , i.e., $\|\mathbf{M}\|_{2 \rightarrow \infty}$ is the maximum of the ℓ_2 norms of the rows of \mathbf{M} . We note that the two-to-infinity norm is *not* sub-multiplicative. However, for any matrices \mathbf{M} and \mathbf{N} of conformal dimensions, we have

$$\|\mathbf{MN}\|_{2 \rightarrow \infty} \leq \min\{\|\mathbf{M}\|_{2 \rightarrow \infty} \times \|\mathbf{N}\|, \|\mathbf{M}\|_\infty \times \|\mathbf{N}\|_{2 \rightarrow \infty}\};$$

see Proposition 6.5 in [Cape et al. \[2019\]](#). Perturbation bounds using the two-to-infinity norm for the eigenvectors and/or singular vectors of a noisily observed matrix had recently attracted interests from the statistics community, see e.g., [Abbe et al. \[2020\]](#), [Cape et al. \[2019\]](#), [Chen et al. \[2021\]](#), [Damle and Sun \[2020\]](#), [Fan et al. \[2018\]](#), [Lei \[2019\]](#) and the references therein.

2 Model

Our model for pairs of random networks is based on the concept of the random dot product graph (RDPG) [\[Athreya et al., 2018, Young and Scheinerman, 2007\]](#).

Definition 1 (Random dot product graph (RDPG)). *Let $d \geq 1$ be given and let \mathcal{X} be a subset of \mathbb{R}^d such that $x^\top y \in [0, 1]$ for any $x, y \in \mathcal{X}$. For a given $n \geq 1$, let $\mathbf{X} = [\mathbf{x}_1, \mathbf{x}_2, \dots, \mathbf{x}_n]^\top$ be a $n \times d$ matrix with $\mathbf{x}_k \in \mathcal{X}$ for all $k \in [n]$. A random network G is said to be a random dot product graph with latent positions of the vertices in \mathbf{X} , where each row $\mathbf{x}_k \in \mathbb{R}^d$ denotes the latent position for the k th vertex, if the adjacency matrix \mathbf{A} of G is a symmetric matrix whose upper triangular entries $\{\mathbf{A}_{s,t}\}_{s < t}$ are independent Bernoulli random variables with*

$$\mathbf{A}_{s,t} \sim \text{Bernoulli}(\mathbf{x}_s^\top \mathbf{x}_t).$$

We define $\mathbf{P} := \mathbf{X}\mathbf{X}^\top$ as the connection probability matrix of G and denote such a graph by $\text{RDPG}(\mathbf{X}\mathbf{X}^\top)$. In this case, the success probabilities of $\{\mathbf{A}_{s,t}\}_{s<t}$ are given by $\mathbf{P}_{s,t} = \mathbf{x}_s^\top \mathbf{x}_t$.

Remark 1 (Orthogonal nonidentifiability in RDPGs). *Note that if $G \sim \text{RDPG}(\mathbf{X}\mathbf{X}^\top)$ with the latent position matrix $\mathbf{X} \in \mathbb{R}^{n \times d}$, then for any orthogonal matrix $\mathbf{W} \in \mathcal{O}_d$, $\mathbf{X}\mathbf{W}$ also gives rise to an RDPG with the same probability distribution, as the connection probability matrix $\mathbf{P} = \mathbf{X}\mathbf{X}^\top = (\mathbf{X}\mathbf{W})(\mathbf{X}\mathbf{W})^\top$ remains unchanged. Thus, the RDPG model is non-identifiable up to orthogonal transformations.*

The RDPG is a special case of latent position graphs or graphons [Diaconis and Janson, 2008, Hoff et al., 2002, Lovász, 2012]. In the general latent position graph model, each vertex s is associated with a latent or unobserved vector $\mathbf{x}_s \in \mathcal{X}$ where \mathcal{X} is some latent space such as \mathbb{R}^d , and given the collection of latent vectors $\{\mathbf{x}_s\}$, the edges are conditionally independent Bernoulli random variables with success probabilities $\mathbf{P}_{s,t} = \kappa(\mathbf{x}_s, \mathbf{x}_t)$ for some kernel function $\kappa : \mathcal{X} \times \mathcal{X} \rightarrow [0, 1]$. For RDPGs, κ is the inner product.

We consider a pair of networks $G^{(1)}$ and $G^{(2)}$ and assume they are independent RDPGs with latent position matrices $\mathbf{X}^{(1)}$ and $\mathbf{X}^{(2)}$, respectively, i.e., $G^{(i)} \sim \text{RDPG}(\mathbf{X}^{(i)}\mathbf{X}^{(i)\top})$ for $i \in \{1, 2\}$. Furthermore, we assume that a subset of vertices shares latent positions between the two networks, up to some orthonormal transformation. We denote the set of unshifted vertices as $\mathcal{U} \subseteq [n]$ and the set of shifted vertices as its complement, \mathcal{U}^c . That is, there exists $\mathbf{W}^{(1,2)} \in \mathcal{O}_d$ such that

$$\mathbf{X}_{\mathcal{U}}^{(2)} = \mathbf{X}_{\mathcal{U}}^{(1)}\mathbf{W}^{(1,2)}.$$

Notice that the probability submatrices associated with \mathcal{U} are also identical across the two networks, i.e., $\mathbf{P}_{\mathcal{U}\mathcal{U}}^{(1)} = \mathbf{P}_{\mathcal{U}\mathcal{U}}^{(2)}$. We denote the vertex-wise changes in latent positions by $\mathbf{Y} \in \mathbb{R}^{n \times d}$, satisfying

$$\mathbf{X}^{(2)} = \mathbf{X}^{(1)}\mathbf{W}^{(1,2)} + \mathbf{Y}, \tag{1}$$

where $\mathbf{Y}_{\mathcal{U}} = \mathbf{0}$ for the unshifted vertices, and $\mathbf{Y}_{\mathcal{U}^c}$ captures the shifts for the shifted vertices.

Given the observed adjacency matrices $\mathbf{A}^{(1)}$ and $\mathbf{A}^{(2)}$, our goal is to estimate the set of unshifted vertices \mathcal{U} (with the set of shifted vertices \mathcal{U}^c) and the shifts in \mathbf{Y} . The corresponding algorithms are provided in Section 3.

3 Algorithm

Given each observed adjacency matrix $\mathbf{A}^{(i)}$ for $i \in \{1, 2\}$, we first estimate the underlying latent position matrix $\mathbf{X}^{(i)}$ using the scaled leading eigenvectors $\hat{\mathbf{X}}^{(i)} = \hat{\mathbf{U}}^{(i)}(\hat{\mathbf{\Lambda}}^{(i)})^{1/2}$, where $\hat{\mathbf{\Lambda}}^{(i)} \in \mathbb{R}^{d \times d}$ is a diagonal matrix whose diagonal entries are the leading d eigenvalues of $\mathbf{A}^{(i)}$ in descending order, and the orthonormal columns of $\hat{\mathbf{U}}^{(i)} \in \mathbb{R}^{n \times d}$ constitute the corresponding eigenvectors. We now propose algorithms to align $\hat{\mathbf{X}}^{(1)}$ and $\hat{\mathbf{X}}^{(2)}$ in order to estimate the set of unshifted vertices \mathcal{U} and the shifts in \mathbf{Y} .

3.1 Seed-based algorithm

We begin with the case where a seed set $\mathcal{S} \subset \mathcal{U}$ of unshifted vertices is available, with $|\mathcal{S}| \geq d$. Using this seed set, the orthogonal matrix $\hat{\mathbf{W}}^{(1,2)}$ aligning the estimated latent position matrices $\hat{\mathbf{X}}^{(1)}$ and $\hat{\mathbf{X}}^{(2)}$ can be determined by

$$\hat{\mathbf{W}}^{(1,2)} = \arg \min_{\mathbf{O} \in \mathcal{O}_d} \|\hat{\mathbf{X}}_{\mathcal{S}}^{(1)} \mathbf{O} - \hat{\mathbf{X}}_{\mathcal{S}}^{(2)}\|_F.$$

The shifts in \mathbf{Y} are then estimated as

$$\hat{\mathbf{Y}} = \hat{\mathbf{X}}^{(2)} - \hat{\mathbf{X}}^{(1)} \hat{\mathbf{W}}^{(1,2)}.$$

Using the test statistic T_k proposed in Eq. (4), we can test whether each vertex k is unshifted or shifted, i.e., whether $\mathbf{y}_k = \mathbf{0}$ or not, where \mathbf{y}_k is the k th row of \mathbf{Y} , representing the shift for vertex k . Based on the asymptotic distribution result for T_k in Theorem 3, by comparing each T_k with the critical value c_α from the χ_d^2 distribution at the chosen significance level α , we obtain the estimated set of unshifted vertices $\hat{\mathcal{U}}$. See Algorithm 1 for the detailed procedure.

Algorithm 1: Vertex-wise shift learning across networks with seeds.

Input: Adjacency matrices $\mathbf{A}^{(1)}, \mathbf{A}^{(2)} \in \mathbb{R}^{n \times n}$, embedding dimension d , a seed set

$\mathcal{S} \subset [n]$ with $|\mathcal{S}| \geq d$, the significant level α .

1. For each network $i \in \{1, 2\}$, compute the estimated latent position matrix $\hat{\mathbf{X}}^{(i)} = \hat{\mathbf{U}}^{(i)}(\hat{\mathbf{\Lambda}}^{(i)})^{1/2} \in \mathbb{R}^{n \times d}$, where $\hat{\mathbf{\Lambda}}^{(i)} \in \mathbb{R}^{d \times d}$ is a diagonal matrix containing the leading d eigenvalues of $\mathbf{A}^{(i)}$ in descending order, and $\hat{\mathbf{U}}^{(i)} \in \mathbb{R}^{n \times d}$ is the matrix whose columns are the corresponding orthonormal eigenvectors.
2. Obtain the orthogonal transformation $\hat{\mathbf{W}}^{(1,2)} \in \mathcal{O}_d$ to align the estimated latent position matrices by solving the orthogonal Procrustes problem on the seed set \mathcal{S} :

$$\hat{\mathbf{W}}^{(1,2)} = \arg \min_{\mathbf{O} \in \mathcal{O}_d} \|\hat{\mathbf{X}}_{\mathcal{S}}^{(2)} - \hat{\mathbf{X}}_{\mathcal{S}}^{(1)} \mathbf{O}\|_{\text{F}}.$$

3. Obtain the estimated shift matrix as $\hat{\mathbf{Y}} = \hat{\mathbf{X}}^{(2)} - \hat{\mathbf{X}}^{(1)} \hat{\mathbf{W}}^{(1,2)} \in \mathbb{R}^{n \times d}$.

4. For all vertex $k \in [n]$, compute the test statistic T_k as

$$T_k = \hat{\mathbf{y}}_k^\top (\hat{\mathbf{\Gamma}}^{(k)})^{-1} \hat{\mathbf{y}}_k,$$

where $\hat{\mathbf{\Gamma}}^{(k)}$ is a $d \times d$ matrix defined by

$$\begin{aligned} \hat{\mathbf{\Gamma}}^{(k)} &= (\hat{\mathbf{X}}^{(2)\top} \hat{\mathbf{X}}^{(2)})^{-1} \hat{\mathbf{X}}^{(2)\top} \hat{\mathbf{\Xi}}^{(k,2)} \hat{\mathbf{X}}^{(2)} (\hat{\mathbf{X}}^{(2)\top} \hat{\mathbf{X}}^{(2)})^{-1} \\ &\quad + \hat{\mathbf{W}}^{(1,2)\top} (\hat{\mathbf{X}}^{(1)\top} \hat{\mathbf{X}}^{(1)})^{-1} \hat{\mathbf{X}}^{(1)\top} \hat{\mathbf{\Xi}}^{(k,1)} \hat{\mathbf{X}}^{(1)} (\hat{\mathbf{X}}^{(1)\top} \hat{\mathbf{X}}^{(1)})^{-1} \hat{\mathbf{W}}^{(1,2)}, \end{aligned}$$

and for $i = 1, 2$, $\hat{\mathbf{\Xi}}^{(k,i)}$ is an $n \times n$ diagonal matrix with diagonal entries

$$\hat{\mathbf{\Xi}}_{\ell,\ell}^{(k,i)} = \hat{\mathbf{P}}_{k\ell}^{(i)} (1 - \hat{\mathbf{P}}_{k\ell}^{(i)}),$$

where $\hat{\mathbf{P}}^{(i)}$ is the estimated connection probability matrix for network i , computed as $\hat{\mathbf{P}}^{(i)} = \hat{\mathbf{X}}^{(i)} \hat{\mathbf{X}}^{(i)\top}$, with entries adjusted to lie in $[0, 1]$, i.e., $\hat{\mathbf{P}}_{k,\ell}^{(i)} = \min(\max(\hat{\mathbf{P}}_{k,\ell}^{(i)}, 0), 1)$.

5. Obtain the estimated set of unshifted vertices as $\hat{\mathcal{U}} = \{k \in [n] : T_k \leq c_\alpha\}$, where c_α denotes the upper α -quantile of the χ_d^2 distribution.

Output: The estimated set of invariant vertices $\hat{\mathcal{U}}$, the estimated shift matrix $\hat{\mathbf{Y}}$, the test statistics $\{T_k\}_{k \in [n]}$, and the critical value c_α .

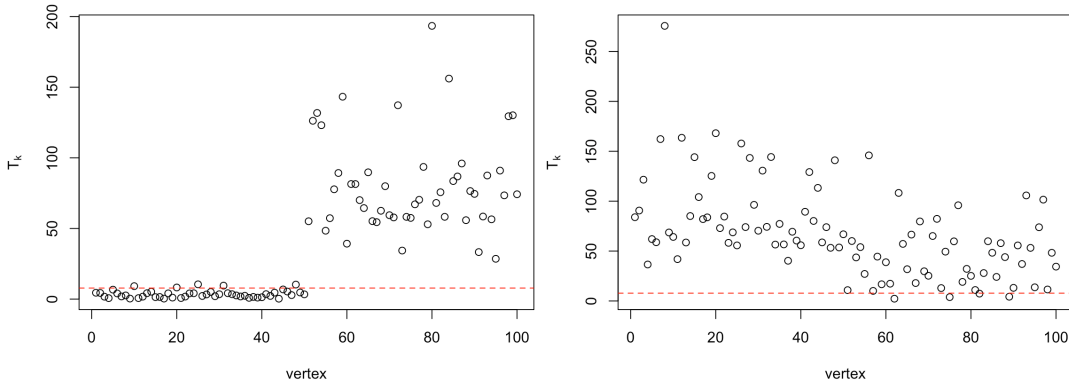
3.2 Seed-free algorithm

In many practical scenarios, a seed set is not available. Building on Algorithm 1, we now propose an algorithm that eliminates the need for a known seed set.

When no seed set is available, our strategy is to guess a correct seed set. The key idea is that if the guessed seed set \mathcal{S} is correct, i.e., $\mathcal{S} \subset \mathcal{U}$, then using Algorithm 1 with this correct \mathcal{S} allows us to determine the accurate orthogonal transformation $\hat{\mathbf{W}}^{(1,2)}$ between $\hat{\mathbf{X}}^{(1)}$ and $\hat{\mathbf{X}}^{(2)}$, and consequently, the estimated set of unshifted vertices $\hat{\mathcal{U}}$, consisting of the aligned vertices via $\hat{\mathbf{W}}^{(1,2)}$, closely approximates the true \mathcal{U} . Conversely, if the guessed seed set \mathcal{S} is incorrect, i.e., $\mathcal{S} \not\subset \mathcal{U}$, Algorithm 1 with this incorrect \mathcal{S} fails to identify the true \mathcal{U} , and in such cases, the number of vertices that can be aligned using an incorrect seed set is typically small, resulting in a small size for the corresponding estimated unshifted set $|\hat{\mathcal{U}}|$.

We illustrate the above idea with a simulation example. Consider two networks on 100 vertices, where the first 50 vertices exhibit no shift while the last 50 vertices experience shifts (i.e., $\mathcal{U} = \{1, 2, \dots, 50\}$); further details about this experiment are provided in Section 5.4. For the case where a correct seed set, such as $\mathcal{S} = \{1, 2, 3\} \subset \mathcal{U}$, is used, the test statistics $\{T_k\}$ for all $n = 100$ vertices, obtained by Algorithm 1, are shown in the left panel of Figure 2. The figure indicates that the test statistics $\{T_k\}$ for the first 50 vertices are mostly below the red dashed line, which represents the critical value c_α . This demonstrates that most unshifted vertices are successfully identified, and the estimated set of unshifted vertices $\hat{\mathcal{U}}$ closely approximates the true \mathcal{U} . Conversely, when an incorrect seed set, such as $\mathcal{S} = \{51, 52, 53\} \not\subset \mathcal{U}$, is used, the test statistics T_k are shown in the right panel of Figure 2. In this case, the true set \mathcal{U} cannot be identified, and the number of aligned vertices, i.e., those with T_k below the critical value c_α , is very small – only 4 vertices in this experiment.

Following this idea, we randomly generate M candidate seed sets, each of size $L \geq d$, and apply Algorithm 1 with each candidate seed set $m \in [M]$ to obtain the corresponding



(a) $\{T_k\}$ obtained using a correct seed set (b) $\{T_k\}$ obtained using an incorrect seed set

Figure 2: The test statistics $\{T_k\}_{k \in [n]}$ are obtained using either a correct seed set $\mathcal{S} = \{1, 2, 3\}$ or an incorrect seed set $\mathcal{S} = \{50, 51, 52\}$. Among the total of $n = 100$ vertices, the first 50 exhibit no shift while the last 50 experience shifts (i.e., $\mathcal{U} = \{1, 2, \dots, 50\}$). The red horizontal dashed line indicates the critical value $c_{\alpha=0.05}$, used to reject the null hypothesis that there is no shift for a given vertex.

set of aligned vertices $\mathcal{U}^{[m]}$. The candidate seed set that yields the largest $\mathcal{U}^{[m]}$ is selected as the most likely correct seed set, denoted by \mathcal{S}^* . Finally, based on \mathcal{S}^* , we can obtain the estimated set of invariant vertices $\hat{\mathcal{U}}$ and the estimated shift matrix $\hat{\mathbf{Y}}$. See Algorithm 2 for the detailed procedure.

To determine the seed set size L and the number of candidate seed sets M for Algorithm 2, the theoretical result in Theorem 1 indicates that our algorithms remain effective even when the seed set size $L = |\mathcal{S}|$ is as small as the minimal dimension d ; see Remark 4 for further discussion. Therefore, to reduce computational cost, we can simply set $L = d$. Next, we consider the appropriate size for M . Suppose the proportion of unshifted vertices is p , i.e., $p = |\mathcal{U}|/n$. Then the probability that a randomly chosen seed vertex belongs to \mathcal{U} is p , and the probability that a randomly generated seed set \mathcal{S} of size $L = d$ is fully contained within \mathcal{U} is approximately p^d . To ensure that at least one candidate seed set is correct with a probability of at least q , it suffices to choose $M \geq \frac{\ln(1-q)}{\ln(1-p^d)}$. For instance, when the latent position dimension $d = 3$ and the proportion of unshifted vertices $p = 1/4$, it is sufficient to set $M \geq 293$ to ensure that at least one candidate seed set is correct with

Algorithm 2: Vertex-wise shift learning across networks without seeds.

Input: Adjacency matrices $\mathbf{A}^{(1)}, \mathbf{A}^{(2)} \in \mathbb{R}^{n \times n}$, embedding dimension d , the size of seed set $L \geq d$, the number of candidate seed sets M , the significant level α , a threshold $\tau > 0$.

1. Apply Step 1 of Algorithm 1 to obtain the estimated latent position matrices $\hat{\mathbf{X}}^{(1)}, \hat{\mathbf{X}}^{(2)} \in \mathbb{R}^{n \times d}$ from $\mathbf{A}^{(1)}$ and $\mathbf{A}^{(2)}$, respectively, for the two networks. Additionally, compute the estimated connection probability matrices $\hat{\mathbf{P}}^{(1)}$ and $\hat{\mathbf{P}}^{(2)}$ using the formulas provided in Step 4 of Algorithm 1, and compute $\Delta = \hat{\mathbf{P}}^{(1)} - \hat{\mathbf{P}}^{(2)}$.
2. Randomly generate M candidate seed sets, each $\mathcal{S}^{[m]} \subset [n]$ with size $|\mathcal{S}^{[m]}| = L$ for all $m \in [M]$.
3. For each candidate seed set $m \in [M]$, if $\|\Delta_{\mathcal{S}^{[m]}, \mathcal{S}^{[m]}}\|_{\max} \leq \tau$, apply Steps 2-5 of Algorithm 1 with $\mathcal{S}^{[m]}$ to obtain the size of the corresponding estimated set of unshifted vertices, $h^{[m]} = |\hat{\mathcal{U}}|$; otherwise, set $h^{[m]} = 0$.
4. Select the most likely correct seed set $\mathcal{S}^* = \mathcal{S}^{[m^*]}$, where

$$m^* = \arg \max_{m \in [M]} h^{[m]}.$$

5. Apply Steps 2-5 of Algorithm 1 with the seed set \mathcal{S}^* to obtain the corresponding estimated set of unshifted vertices \mathcal{U}^* . Update $\mathcal{S}^* = \mathcal{U}^*$ to expand the seed set. Finally, rerun Steps 2-5 of Algorithm 1 with the updated seed set \mathcal{S}^* to produce the final output.

Output: The estimated set of invariant vertices $\hat{\mathcal{U}}$, the estimated shift matrix $\hat{\mathbf{Y}}$, the test statistics $\{T_k\}_{k \in [n]}$, and the critical value c_α .

a probability of at least $q = 0.99$. Therefore, in many practical scenarios, choosing M on the order of a few thousand is typically sufficient to guarantee robust performance.

To further reduce computational complexity, we introduce a filtering step in Step 3 of Algorithm 2 for the randomly generated seed sets. Observing that the underlying probability submatrices associated with the unshifted vertex set \mathcal{U} are identical across the two networks, i.e., $\mathbf{P}_{\mathcal{U},\mathcal{U}}^{(1)} = \mathbf{P}_{\mathcal{U},\mathcal{U}}^{(2)}$, their estimates are expected to satisfy $\hat{\mathbf{P}}_{\mathcal{U},\mathcal{U}}^{(1)} \approx \hat{\mathbf{P}}_{\mathcal{U},\mathcal{U}}^{(2)}$, i.e., $\Delta_{\mathcal{U},\mathcal{U}} \approx \mathbf{0}$ for $\Delta = \hat{\mathbf{P}}^{(1)} - \hat{\mathbf{P}}^{(2)}$. Thus for a correct seed set $\mathcal{S} \subset \mathcal{U}$, we also expect $\Delta_{\mathcal{S},\mathcal{S}} \approx \mathbf{0}$, and to enforce this, we filter candidate seed sets using a threshold τ , such as 0.3 or 0.5, by retaining only those sets satisfying $\|\Delta_{\mathcal{S},\mathcal{S}}\|_{\max} \leq \tau$. Seed sets passing this criterion are retained for further computation of $h^{[m]}$. This filtering step significantly reduces the number of candidate seed sets requiring full evaluation, thereby improving computational efficiency while maintaining accuracy.

Note that in Step 5 of Algorithm 2, we expand the selected seed set of size L to a larger seed set before producing the final output. This step is motivated by the theoretical result in Theorem 1, which indicates that while the minimal size d is sufficient, especially when n is large enough, an increased seed set size can improve the accuracy of the estimates.

Finally, we discuss how to choose the embedding dimension d in practice. We can examine the eigenvalues of the adjacency matrices, and an ubiquitous and principled method is to examine the so-called scree plot and look for “elbow” and “knees” defining the cut-off between the top (signal) d dimension and the noise dimensions. [Zhu and Ghodsi \[2006\]](#) provide an automatic dimensionality selection procedure to look for the “elbow” by maximizing a profile likelihood function. [Han et al. \[2023\]](#) suggest another universal approach to rank inference via residual subsampling for estimating the rank. Other related methods include the eigenvalue ratio test [[Ahn and Horenstein, 2013](#)] and techniques based on the empirical distribution of eigenvalues [[Onatski, 2010](#)].

3.3 Computational complexity

We now describe the computational complexity of our proposed algorithms. For Algorithm 1, the embedding step in Step 1 has a complexity of roughly $O(n^2d)$ [Huffel, 1990]; the orthogonal Procrustes problem on the seed set of size $|\mathcal{S}|$ in Step 2 has a complexity of approximately $O(|\mathcal{S}|d^2)$; Steps 3-5 require some matrix operations and its complexity is roughly $O(n^2d)$. Thus the overall computational complexity of Algorithm 1 is $O(n^2d)$. Note that the embedding dimension d is typically bounded while the number of vertices n determines the primary computational cost.

For Algorithm 2, its Step 1 involves Steps 1 and 4 of Algorithm 1, with a complexity of is $O(n^2d)$; the random generation procedure in its Step 2 has a complexity of $O(LM)$; Step 3 involves applying Algorithm 1 and has a complexity of $O(Mn^2d)$; the selection of the optimal seed set in Step 4 has a complexity of $O(M)$; Step 5 again applies Algorithm 1 and has a complexity of $O(n^2d)$. Hence the overall computational complexity of Algorithm 2 is $O(Mn^2d)$. And according to the discussion in Section 3.2, the number of candidate seed sets M is typically sufficient in the range of several hundred to a few thousand.

Empirically, we record the running time of the simulation experiments described in Section 5.4 for n ranging from 50 to 800 vertices, as shown in the right panel of Figure 7. From Figure 7, the running time of Algorithm 2 scales approximately quadratically with n , consistent with the theoretical analysis above. Furthermore, even for $n = 800$ demonstrating exceptional robustness and precision, the running time on a standard computer for 100 Monte Carlo replicates is only about 22 minutes.

4 Theoretical Results

For each rank- d probability matrix $\mathbf{P}^{(i)} = \mathbf{X}^{(i)}\mathbf{X}^{(i)\top}$ for $i = 1, 2$, we denote the eigen-decomposition of $\mathbf{P}^{(i)}$ by $\mathbf{P}^{(i)} = \mathbf{U}^{(i)}\mathbf{\Lambda}^{(i)}\mathbf{U}^{(i)\top}$, where $\mathbf{\Lambda}^{(i)} \in \mathbb{R}^{d \times d}$ is a diagonal matrix containing the d eigenvalues of $\mathbf{P}^{(i)}$ in descending order, and $\mathbf{U}^{(i)} \in \mathbb{R}^{n \times d}$ is a matrix

whose orthonormal columns are the corresponding eigenvectors. For ease of exposition, in the theoretical analysis we assume $\mathbf{X}^{(i)} = \mathbf{U}^{(i)}(\mathbf{\Lambda}^{(i)})^{1/2}$. Generally $\mathbf{X}^{(i)}$ may differ from $\mathbf{U}^{(i)}(\mathbf{\Lambda}^{(i)})^{1/2}$ by an orthogonal matrix, which only involves some book-keeping but does not affect the essence of any theoretical results.

We shall make the following assumptions on the probability matrices $\mathbf{P}^{(1)}, \mathbf{P}^{(2)} \in \mathbb{R}^{n \times n}$. We emphasize that, because our theoretical results address either large-sample approximations or limiting distributions, these assumptions should be interpreted in the regime where n is arbitrarily large and/or $n \rightarrow \infty$.

Assumption 1. *The following conditions hold for sufficiently large n .*

- $\{\mathbf{U}^{(i)}\}$ are $n \times d$ matrices with bounded coherence, i.e.,

$$\|\mathbf{U}^{(i)}\|_{2 \rightarrow \infty} \lesssim d^{1/2} n^{-1/2}.$$

- There exists a factor $\rho_n \in [0, 1]$ depending on n such that for each $i = 1, 2$, $\|\mathbf{\Lambda}^{(i)}\| = \Theta(n\rho_n)$ where $n\rho_n = \Omega(\log n)$. We interpret $n\rho_n$ as the growth rate for the average degree of the networks $\{\mathbf{A}^{(i)}\}$ generated from $\{\mathbf{P}^{(i)}\}$.

- $\{\mathbf{P}^{(i)}\}$ have bounded condition numbers, i.e., there exists a finite constant $M > 0$ such that

$$\max_{i=1,2} \frac{\lambda_1(\mathbf{\Lambda}^{(i)})}{\lambda_d(\mathbf{\Lambda}^{(i)})} \leq M,$$

where $\lambda_1(\mathbf{\Lambda}^{(i)})$ and $\lambda_d(\mathbf{\Lambda}^{(i)})$ denote the largest and smallest non-zero eigenvalues of $\mathbf{P}^{(i)}$, respectively.

- For the seed set \mathcal{S} , the latent position matrix $\mathbf{X}_{\mathcal{S}}^{(2)} = \mathbf{X}_{\mathcal{S}}^{(1)} \mathbf{W}^{(1,2)}$ achieves rank d , and we suppose

$$(\sigma_d(\mathbf{X}_{\mathcal{S}}^{(1)}))^2 = \lambda_d(\mathbf{P}_{\mathcal{S},\mathcal{S}}^{(1)}) \gtrsim \frac{|\mathcal{S}|}{n} \lambda_d(\mathbf{P}^{(1)});$$

see Remark 2 for more discussion for this condition.

Remark 2. *The assumption on $\lambda_d(\mathbf{P}_{\mathcal{S},\mathcal{S}})$ holds with high probability when \mathcal{S} is drawn uniformly at random from \mathcal{U} ; see Lemma D.11 in Zheng and Tang [2024], consistent with the seed set generation method in Algorithm 2. Theoretical results under weaker assumptions on it or even without such assumptions can also be derived following our analysis.*

Remark 3. *The remaining conditions in Assumption 1 are quite mild and typically seen in the literature. The first condition on bounded coherence and the third condition on bounded condition number are prevalent and typically mild in random networks and many other high-dimensional statistics inference problems including matrix completion, covariance estimation, and subspace estimation, see e.g.. Abbe et al. [2020], Cai et al. [2021], Candes and Recht [2009], Cape et al. [2019], Chen et al. [2021], Fan et al. [2018], Lei [2019]. The second condition $\|\mathbf{P}^{(i)}\| \asymp n\rho_n = \Omega(\log n)$ implies that the average degree of each network $\mathbf{A}^{(i)}$ grows poly-logarithmically in n , and this semi-sparse regime $n\rho_n = \Omega(\log n)$ is generally necessary for spectral methods to work [Xie, 2024].*

We now establish uniform error bounds and provide normal approximations for the row-wise fluctuations of the estimated shift matrix $\hat{\mathbf{Y}}$ obtained based on a given seed set \mathcal{S} around the true shift matrix \mathbf{Y} .

Theorem 1. *Let the adjacency matrices $\mathbf{A}^{(1)} \sim \text{RDPG}(\mathbf{X}^{(1)}\mathbf{X}^{(1)\top})$ and $\mathbf{A}^{(2)} \sim \text{RDPG}(\mathbf{X}^{(2)}\mathbf{X}^{(2)\top})$, where $\mathbf{X}^{(2)} = \mathbf{X}^{(1)}\mathbf{W}^{(1,2)} + \mathbf{Y}$ with some $\mathbf{W}^{(1,2)} \in \mathcal{O}_d$ and the shift matrix \mathbf{Y} satisfying $\mathbf{Y}_{\mathcal{U}} = \mathbf{0}$ for the set of unshifted vertices \mathcal{U} . Let the probability matrices $\mathbf{P}^{(i)} = \mathbf{X}^{(i)}\mathbf{X}^{(i)\top}$ and the seed set $\mathcal{S} \subset \mathcal{U}$ satisfy the conditions in Assumption 1. We obtain the estimated orthogonal transformation as*

$$\hat{\mathbf{W}}^{(1,2)} = \arg \min_{\mathbf{O} \in \mathcal{O}_d} \|\hat{\mathbf{X}}_{\mathcal{S}}^{(1)}\mathbf{O} - \hat{\mathbf{X}}_{\mathcal{S}}^{(2)}\|_F,$$

and then compute the estimated shift matrix as

$$\hat{\mathbf{Y}} = \hat{\mathbf{X}}^{(2)} - \hat{\mathbf{X}}^{(1)}\hat{\mathbf{W}}^{(1,2)}.$$

Then there exists $\mathbf{W} \in \mathcal{O}_d$ such that

$$\hat{\mathbf{Y}}\mathbf{W} - \mathbf{Y} = \mathbf{E}^{(2)}\mathbf{X}^{(2)}(\mathbf{X}^{(2)\top}\mathbf{X}^{(2)})^{-1} - \mathbf{E}^{(1)}\mathbf{X}^{(1)}(\mathbf{X}^{(1)\top}\mathbf{X}^{(1)})^{-1}\mathbf{W}^{(1,2)} + \mathbf{R},$$

where $\mathbf{E}^{(i)} = \mathbf{A}^{(i)} - \mathbf{P}^{(i)}$ and \mathbf{R} is a $n \times d$ matrix satisfying

$$\|\mathbf{R}\|_{2 \rightarrow \infty} \lesssim |\mathcal{S}|^{-1/2} n^{-1/2} \log^{1/2} n + n^{-1/2} (n\rho_n)^{-1/2} \log n$$

with high probability, and we further have

$$\|\hat{\mathbf{Y}}\mathbf{W} - \mathbf{Y}\|_{2 \rightarrow \infty} \lesssim n^{-1/2} \log^{1/2} n$$

with high probability.

Remark 4. We first note that Theorem 1 has no requirements on the size of the seed set, $|\mathcal{S}|$, and the error rate for $\|\hat{\mathbf{Y}}\mathbf{W} - \mathbf{Y}\|_{2 \rightarrow \infty}$ decreases as n increases, not depending on $|\mathcal{S}|$; see Section 5.3 for the corresponding simulation. This implies that our algorithms remain effective even when $|\mathcal{S}|$ is as small as the minimal d , which is the smallest seed set size necessary for aligning the d -dimensional latent positions. Therefore, in the step of Algorithm 2 where a correct seed set is guessed, we can reduce computational cost by selecting only $|\mathcal{S}| = d$ seeds.

In addition, Theorem 1 also shows that a increase in $|\mathcal{S}|$ may lead to a further reduction in the error term $\|\mathbf{R}\|_{2 \rightarrow \infty}$. This observation motivates a enhancement to the final step of Algorithm 2: using all detected unshifted vertices as a new, larger seed set to replace the original seed set, and then rerunning Algorithm 1 to obtain the final estimate.

Theorem 2. Consider the setting in Theorem 1. Further assume that $\mathbf{A}^{(1)}$ and $\mathbf{A}^{(2)}$ are independent, $n\rho_n = \omega(\log^2 n)$, and $|\mathcal{S}| = \omega(\log n)$. Then for any $k \in [n]$, let $\Xi^{(k,i)}$ for $i = 1, 2$ be $n \times n$ diagonal matrix whose diagonal entries are of the form

$$\Xi_{\ell,\ell}^{(k,i)} = \mathbf{P}_{k\ell}^{(i)}(1 - \mathbf{P}_{k\ell}^{(i)}).$$

Define $\mathbf{\Gamma}^{(k)}$ as the $d \times d$ symmetric matrix

$$\begin{aligned} \mathbf{\Gamma}^{(k)} &:= (\mathbf{X}^{(2)\top} \mathbf{X}^{(2)})^{-1} \mathbf{X}^{(2)\top} \mathbf{\Xi}^{(k,2)} \mathbf{X}^{(2)} (\mathbf{X}^{(2)\top} \mathbf{X}^{(2)})^{-1} \\ &\quad + \mathbf{W}^{(1,2)\top} (\mathbf{X}^{(1)\top} \mathbf{X}^{(1)})^{-1} \mathbf{X}^{(1)\top} \mathbf{\Xi}^{(k,1)} \mathbf{X}^{(1)} (\mathbf{X}^{(1)\top} \mathbf{X}^{(1)})^{-1} \mathbf{W}^{(1,2)}. \end{aligned}$$

Note that $\|\mathbf{\Gamma}^{(k)}\| \lesssim n^{-1}$, and suppose $\lambda_{\min}(\mathbf{\Gamma}^{(k)}) \gtrsim n^{-1}$. Then for the k th rows $\hat{\mathbf{y}}_k$ of $\hat{\mathbf{Y}}$ and \mathbf{y}_k of \mathbf{Y} we have

$$(\mathbf{\Gamma}^{(k)})^{-1/2} (\mathbf{W}^\top \hat{\mathbf{y}}_k - \mathbf{y}_k) \rightsquigarrow \mathcal{N}(\mathbf{0}, \mathbf{I})$$

as $n \rightarrow \infty$.

Remark 5. The theoretical results and corresponding algorithms can be extended to the setting where $\mathbf{A}^{(1)}$ and $\mathbf{A}^{(2)}$ are correlated. In this case, the expansion in Theorem 1 remains valid, and some normal approximation result like Theorem 2 can still hold but the covariance matrix $\mathbf{\Gamma}^{(k)}$ should be adjusted to account for the correlation between $\mathbf{E}^{(1)}$ and $\mathbf{E}^{(2)}$.

4.1 Testing $\mathbb{H}_0 : \mathbf{y}_k = \mathbf{0}$

We next address the problem of determining whether the latent position of a vertex is shifted, specifically testing the null hypothesis $\mathbb{H}_0 : \mathbf{y}_k = \mathbf{0}$ against the alternative $\mathbb{H}_a : \mathbf{y}_k \neq \mathbf{0}$ for a fixed $k \in [n]$. We now transform the normal approximations for $\hat{\mathbf{Y}}$ established in Theorem 2, into a test statistic for this hypothesis test. Suppose the null hypothesis $\mathbb{H}_0 : \mathbf{y}_k = \mathbf{0}$ is true. Then by Theorem 2 we have

$$\hat{\mathbf{y}}_k^\top \mathbf{W} (\mathbf{\Gamma}^{(k)})^{-1} \mathbf{W}^\top \hat{\mathbf{y}}_k \rightsquigarrow \chi_d^2 \tag{2}$$

as $n \rightarrow \infty$. Our objective is to convert Eq. (2) into a test statistic that depends only on estimates. We first define $\hat{\mathbf{\Gamma}}^{(k)}$ as

$$\begin{aligned} \hat{\mathbf{\Gamma}}^{(k)} &:= (\hat{\mathbf{X}}^{(2)\top} \hat{\mathbf{X}}^{(2)})^{-1} \hat{\mathbf{X}}^{(2)\top} \hat{\mathbf{\Xi}}^{(k,2)} \hat{\mathbf{X}}^{(2)} (\hat{\mathbf{X}}^{(2)\top} \hat{\mathbf{X}}^{(2)})^{-1} \\ &\quad + \hat{\mathbf{W}}^{(1,2)\top} (\hat{\mathbf{X}}^{(1)\top} \hat{\mathbf{X}}^{(1)})^{-1} \hat{\mathbf{X}}^{(1)\top} \hat{\mathbf{\Xi}}^{(k,1)} \hat{\mathbf{X}}^{(1)} (\hat{\mathbf{X}}^{(1)\top} \hat{\mathbf{X}}^{(1)})^{-1} \hat{\mathbf{W}}^{(1,2)}, \end{aligned} \tag{3}$$

where $\hat{\mathbf{\Xi}}^{(k,i)}$ be an $n \times n$ diagonal matrix with diagonal entries defined as $\hat{\mathbf{\Xi}}_{\ell,\ell}^{(k,i)} = \hat{\mathbf{P}}_{k\ell}^{(i)} (1 - \hat{\mathbf{P}}_{k\ell}^{(i)})$; here $\hat{\mathbf{P}}_{k\ell}^{(i)}$ represents the estimated connection probability between vertex k and vertex

ℓ in the network i and we set $\hat{\mathbf{P}}^{(i)} = \hat{\mathbf{X}}^{(i)}\hat{\mathbf{X}}^{(i)\top}$. The following lemma shows that $(\hat{\mathbf{\Gamma}}^{(k)})^{-1}$ is a consistent estimate of $\mathbf{W}(\mathbf{\Gamma}^{(k)})^{-1}\mathbf{W}^\top$.

Lemma 1. *Consider the setting of Theorem 2. We then have*

$$n^{-1}\|\mathbf{W}(\mathbf{\Gamma}^{(k)})^{-1}\mathbf{W}^\top - (\hat{\mathbf{\Gamma}}^{(k)})^{-1}\| \lesssim (n\rho_n)^{-1/2} \log^{1/2} n$$

with high probability.

Given Lemma 1, the following result provides a test statistic for $\mathbb{H}_0 : \mathbf{y}_k = \mathbf{0}$ that converges to a central (resp. non-central) χ^2 under the null (resp. local alternative) hypothesis.

Theorem 3. *Consider the setting in Theorem 2. Define the test statistic*

$$T_k = \hat{\mathbf{y}}_k^\top (\hat{\mathbf{\Gamma}}^{(k)})^{-1} \hat{\mathbf{y}}_k, \quad (4)$$

where $\hat{\mathbf{\Gamma}}^{(k)}$ is given in Eq. (3). Then under $\mathbb{H}_0 : \mathbf{y}_k = \mathbf{0}$, we have

$$T_k \rightsquigarrow \chi_d^2$$

as $n \rightarrow \infty$. Next suppose that $\eta > 0$ is a finite constant and that $\mathbf{y}_k \neq \mathbf{0}$ satisfies a local alternative hypothesis where $\mathbf{y}_k^\top (\mathbf{\Gamma}^{(k)})^{-1} \mathbf{y}_k \rightarrow \eta$. We then have $T_k \rightsquigarrow \chi_d^2(\eta)$ as $n \rightarrow \infty$, where $\chi_d^2(\eta)$ is the non-central chi-square distribution with d degrees of freedom and noncentrality parameter η .

Theorem 3 indicates that, for a chosen significance level α , we reject $\mathbb{H}_0 : \mathbf{y}_k = \mathbf{0}$ if $T_k > c_\alpha$, where c_α is the upper α -quantile of the χ_d^2 distribution, and provides the theoretical foundation for our algorithms.

5 Simulation Experiments

We now present simulation experiments to complement our theoretical results and showcase the performance of our algorithms.

5.1 Estimation error of shifts

We consider two RDPGs on $n = 2000$ vertices, where the latent positions of half the vertices are shifted between them, and the dimension of their latent positions is $d = 3$. The two networks share the latent positions for the first 1000 vertices, and the latent positions in $\mathbf{X}_{\mathcal{U}}^{(1)} = \mathbf{X}_{\mathcal{U}}^{(2)}$, where $\mathcal{U} = \{1, 2, \dots, 1000\}$, are independently and randomly generated. Specifically, we first uniformly generate values between 0 and 1, then take their square root and divide by \sqrt{d} , which ensures that the values in the resulting probability matrix fall between 0 and 1. We use the same procedure to separately generate the latent positions of their distinct last 1000 vertices, $\mathbf{X}_{\mathcal{U}^c}^{(1)}$ and $\mathbf{X}_{\mathcal{U}^c}^{(2)}$, where $\mathcal{U}^c = \{1001, \dots, 2000\}$. In this setting, $\mathbf{Y} = \mathbf{X}^{(2)} - \mathbf{X}^{(1)}$ with the shift $\mathbf{Y}_{\mathcal{U}^c} = \mathbf{X}_{\mathcal{U}^c}^{(2)} - \mathbf{X}_{\mathcal{U}^c}^{(1)}$ and $\mathbf{Y}_{\mathcal{U}} = \mathbf{0}$. We then simulate adjacency matrices $\mathbf{A}^{(1)}$ and $\mathbf{A}^{(2)}$ using the edge probability matrices $\mathbf{P}^{(1)} = \mathbf{X}^{(1)}\mathbf{X}^{(1)\top}$ and $\mathbf{P}^{(2)} = \mathbf{X}^{(2)}\mathbf{X}^{(2)\top}$. Given $\mathbf{A}^{(1)}$ and $\mathbf{A}^{(2)}$, we estimate \mathbf{Y} with the seed set $\mathcal{S} = \{1, 2, \dots, 100\}$ by Algorithm 1.

We repeat the above steps for 1000 Monte Carlo iterations to obtain an empirical distribution of the estimation error $\mathbf{W}^\top \hat{\mathbf{y}}_k - \mathbf{y}_k$ for $k = 1$ which we then compare against the limiting distribution given in Theorem 2. The results are summarized in Figure 3 and Figure 4. Henze-Zirkler’s normality test indicates that the empirical distribution of $\mathbf{W}^\top \hat{\mathbf{y}}_k - \mathbf{y}_k$ is well-approximated by a multivariate normal distribution and furthermore the empirical covariances for $\mathbf{W}^\top \hat{\mathbf{y}}_k - \mathbf{y}_k$ are very close to the theoretical covariances.

5.2 Test statistics for $\mathbb{H}_0 : \mathbf{y}_k = \mathbf{0}$

Under the setting described in Section 5.1, we test $\mathbb{H}_0 : \mathbf{y}_k = \mathbf{0}$ against $\mathbb{H}_a : \mathbf{y}_k \neq \mathbf{0}$ for an unshifted vertex ($k = 1$) and a shifted vertex ($k = 1001$), respectively. The vertex $k = 1$, which retains the same latent position in both networks, corresponds to the null hypothesis, while the vertex $k = 1001$, whose latent position shifts between the two networks, corresponds to the local alternative hypothesis. For each Monte Carlo replicate, we compute the

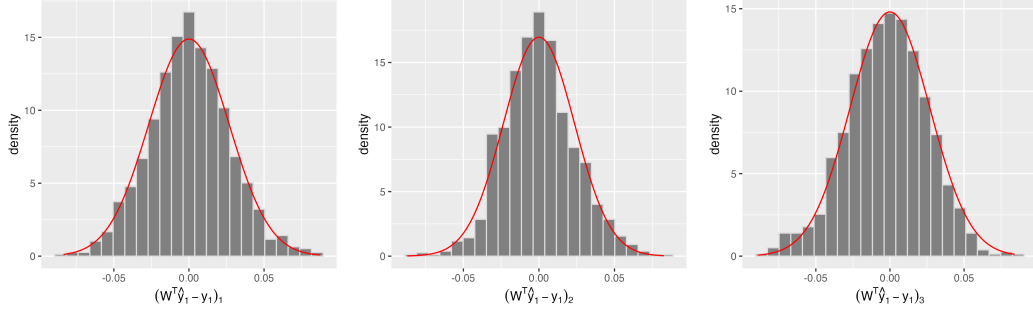


Figure 3: Histograms of the empirical distributions of the entries of the estimation error $\mathbf{W}^\top \hat{\mathbf{y}}_k - \mathbf{y}_k$ for $k = 1$. These histograms are based on 1000 independent Monte Carlo replicates of two RDPGs on $n = 2000$ vertices with $d = 3$ dimensional latent positions, where half of the vertices are shifted. The red lines represent the probability density functions of the normal distributions with parameters specified in Theorem 2.

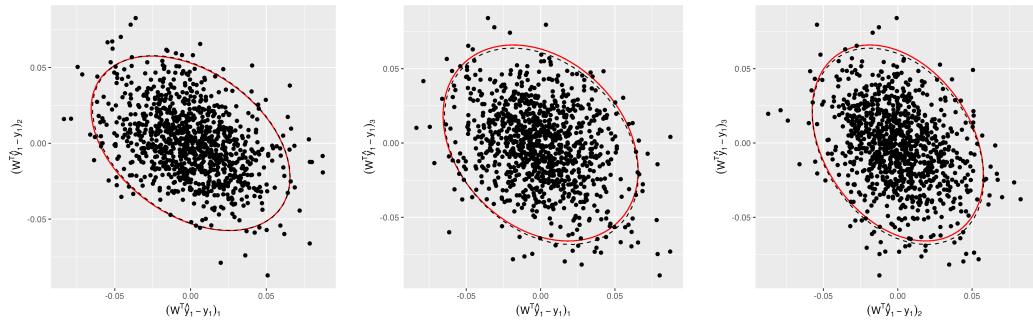


Figure 4: Bivariate plots for the empirical distributions between the entries of the estimation error $\mathbf{W}^\top \hat{\mathbf{y}}_k - \mathbf{y}_k$ for $k = 1$ based on 1000 Monte Carlo replicates of the same setting with Figure 3. Dashed black ellipses represent 95% level curves for the empirical distributions while solid red ellipses represent 95% level curves for the theoretical distributions as specified in Theorem 2.

test statistic T_k from Theorem 3 and compare its empirical distributions under the null and alternative hypotheses to the central and non-central χ^2 distributions with $d = 3$ degrees of freedom. The results, summarized in Figure 5, show that the empirical distributions of T_k are well approximated by the theoretical distributions.

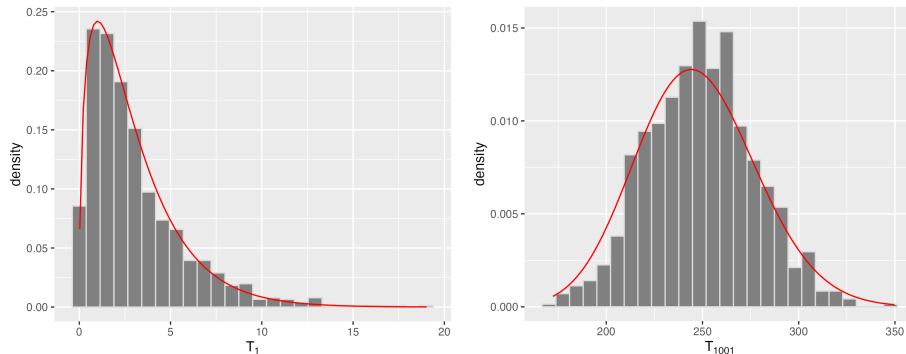


Figure 5: Histograms of the empirical distributions of T_k for an unshifted vertex ($k = 1$) and a shifted vertex ($k = 1001$), corresponding to the null and local alternative hypotheses, respectively. The histograms are based on 1000 independent Monte Carlo replicates of two RDPGs on $n = 2000$ vertices with $d = 3$ dimensional latent positions, where half of the vertices are shifted. The red lines are the probability density functions for the central and non-central chi-square distributions with $d = 3$ degrees of freedom and non-centrality parameters given in Theorem 3.

5.3 Performance with limited seeds

Remark 4 states that, according to Theorem 1, our algorithms remain effective even when the seed set size $|\mathcal{S}|$ is consistently as small as the embedding dimension d , which is the minimal size that can be used. And according to Theorem 1, the estimation error of the shift \mathbf{Y} in terms of the $2 \rightarrow \infty$ norm decreases at a rate of $n^{-1/2} \log^{1/2} n$, regardless of $|\mathcal{S}|$. To validate the results, we conduct simulations using the same settings of two RDPGs as in Section 5.1, but with the number of vertices n varying. The first half of the vertices consistently exhibit no shift, i.e., $\mathcal{U} = \{1, 2, \dots, n/2\}$, while the second half of the vertices are shifted, i.e., $\mathcal{U}^c = \{n/2 + 1, n/2 + 2, \dots, n\}$. We compute the estimation error $\min_{\mathbf{W} \in \mathcal{O}_d} \|\hat{\mathbf{Y}}\mathbf{W} - \mathbf{Y}\|_{2 \rightarrow \infty}$ for several values of n , while fixing the seed set size $|\mathcal{S}| = d = 3$

($\mathcal{S} = \{1, 2, 3\}$). The results are summarized in Figure 6, and note that the slope of the line of Figure 6 approximately matches the theoretical error rate of $n^{-1/2} \log^{1/2} n$ in Theorem 1. In summary, our algorithms can estimate the shifts accurately even with very limited seeds.

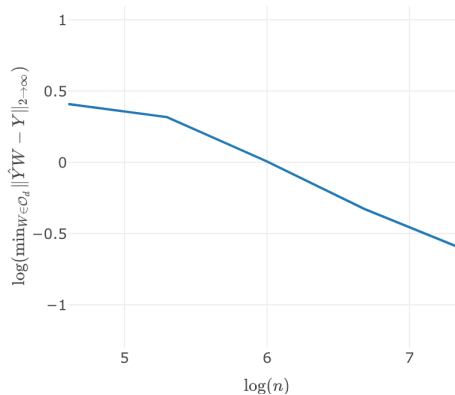


Figure 6: The log-log plot of the empirical error rate of $\min_{\mathbf{W} \in \mathcal{O}_d} \|\hat{\mathbf{Y}}\mathbf{W} - \mathbf{Y}\|_{2 \rightarrow \infty}$ as we vary the number of vertices $n \in \{100, 200, 400, 800, 1600\}$ while fixing the seed set size $|\mathcal{S}| = d = 3$. The errors are based on 100 independent Monte Carlo replicates of two RDPGs on n vertices with d dimensional latent positions, where half of the vertices are shifted.

5.4 Detection of shifted vertices without seeds

We now explore the performance of Algorithm 2 in the case where no seeds are available. Recall that in a stochastic block model (SBM) [Holland et al., 1983] with n vertices and d blocks, the probability matrix is given by $\mathbf{P} = \mathbf{Z}\mathbf{B}\mathbf{Z}^\top$, where $\mathbf{Z} \in \mathbb{R}^{n \times d}$, with entries in $\{0, 1\}$ satisfying $\sum_{k=1}^d \mathbf{Z}_{s,k} = 1$ for all $s \in [n]$, represents the block assignments of the vertices, and $\mathbf{B} \in \mathbb{R}^{d \times d}$, with entries in $[0, 1]$, represents the edge probabilities between blocks. We consider two SBMs in which the block assignments of half of vertices are shifted. We let the block-wise probability matrix

$$\mathbf{B} = \begin{bmatrix} 0.7 & 0.1 & 0.1 \\ 0.1 & 0.65 & 0.1 \\ 0.1 & 0.1 & 0.6 \end{bmatrix},$$

and the block assignments of the vertices are randomly generated. More specifically, the block assignments of the vertices for the first SBM are randomly generated, with each vertex independently assigned to one of the three blocks with equal probability of $1/3$. For the second SBM, the first half of the vertices retain the same block assignments as in the first SBM, i.e., $\mathbf{Z}_{\mathcal{U}}^{(1)} = \mathbf{Z}_{\mathcal{U}}^{(2)}$, where $\mathcal{U} = \{1, 2, \dots, n/2\}$, and the block assignments of the second half of the vertices are changed, with each shifted vertex randomly assigned to one of the two remaining blocks (other than its original block in the first SBM) with equal probability of $1/2$, which means $\mathbf{Z}_{\mathcal{U}^c}^{(1)} = \mathbf{Z}_{\mathcal{U}^c}^{(2)}$, where $\mathcal{U}^c = \{n/2 + 1, n/2 + 2, \dots, n\}$.

Assuming no prior knowledge of the unshifted vertices, we apply Algorithm 2 to detect which vertices are shifted and which are unshifted. The performance is then evaluated using accuracy, which is defined as the proportion of vertices correctly classified as shifted or unshifted out of the total number of vertices. Figure 7 presents the accuracy results and running time as n varies in $\{50, 80, 100, 200, 400, 800\}$, while the parameters of Algorithm 2 are set to $L = 3$, $M = 1000$, $\alpha = 0.05$, and $\tau = 0.3$. It demonstrates that Algorithm 2 is both highly accurate, achieving high detection accuracy with as few as just $n = 80$ vertices, and computationally efficient, requiring only about 2 minutes per Monte Carlo replicate on a standard computer even when $n = 800$.

6 Real Data Experiments

In this section, we apply our algorithms to analyze real datasets, including comparing the brain networks of ADHD patients and controls to detect key brain regions associated with ADHD, as well as analyzing the dynamic chocolate trading network to identify countries with changes in trading patterns over time.

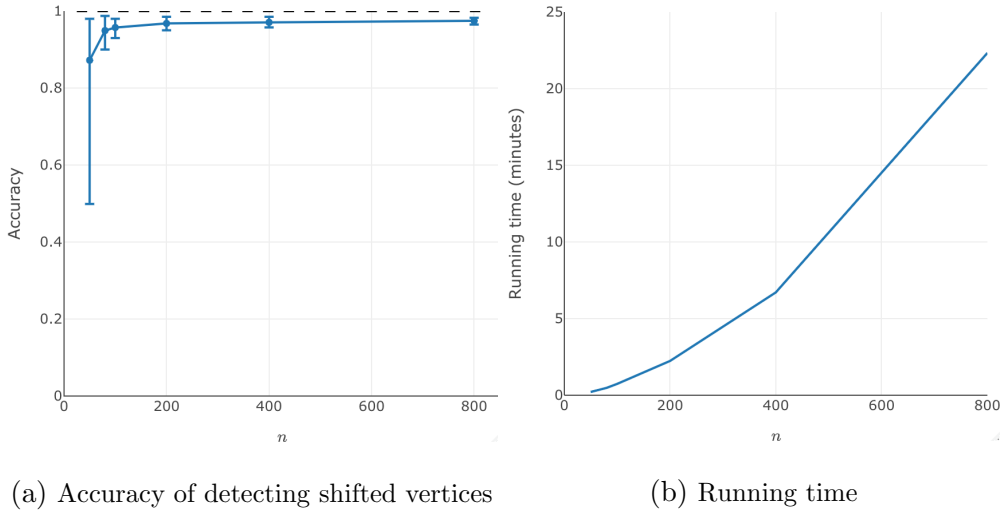


Figure 7: Panel (a) illustrates the accuracy of detecting shifted vertices without seeds, as we vary the number of vertices $n \in \{50, 80, 100, 200, 400, 800\}$ while setting $L = 3$, $M = 1000$, $\alpha = 0.05$, $\tau = 0.3$. Panel (a) reports the mean, along with the 0.05 and 0.95-quantile points, based on 100 independent Monte Carlo replicates of two SBMs on n vertices with $d = 3$ blocks, where the block assignments of half of the vertices are shifted. Panel (b) reports the running time on a standard computer for 100 Monte Carlo replicates.

6.1 Brain networks contrastive study for attention deficit hyperactivity disorder (ADHD)

Attention Deficit Hyperactivity Disorder (ADHD) affects at least 5-10% of school-age children [Polanczyk et al., 2007] and is associated with substantial lifelong impairment. To understand the neurobiological mechanisms underlying ADHD, it is essential to investigate the key brain regions associated with ADHD. In this experiment, we perform our contrastive learning on the brain networks of ADHD patients and healthy controls. By identifying vertices that exhibit significant embedding shifts, we aim to pinpoint the corresponding brain regions that are likely to play critical roles in ADHD, offering insights into its neurobiological basis.

ADHD-200 data is shared through the International Neuroimaging Datasharing Initiative [Mennes et al., 2013], and includes rs-fMRI, structural MRI, and basic information for individuals: some typically-developing controls and patients diagnosed with ADHD [con-

sortium, 2012]. In this experiment, we used the frontal2D dataset from the NBR package [Gracia-Tabuenca and Alcauter, 2020], which was derived from the ADHD200 dataset, with the variables manipulated to differ from the original data. Functional connectivity was measured as the Pearson correlation between the average fMRI signal from the brain regions of interest, i.e., $n = 28$ anatomical areas of the frontal lobe. We consider the total of 17 female individuals in the frontal2D dataset, including 5 ADHD patients and 12 healthy controls.

For any pair of individuals, we can use Algorithm 2 to compare their brain networks and estimate the latent position shifts for all brain regions. To determine the embedding dimension d for Algorithm 2, we apply the automatic dimensionality selection procedure described in Zhu and Ghodsi [2006], and it selects dimensions of 1, 2, and 3 for 4, 9, and 4 networks, respectively, among the total 17 brain networks. Based on this, we choose $d = 3$, as it suffices to capture the complexity of all networks. We set the significance level to detect shifts as $\alpha = 0.01$. The other parameters of Algorithm 2 mainly affect computational complexity, and we choose $L = d = 3$, $M = 5000$, and $\tau = 0.3$

Figure 8 presents a bar chart comparing the differences in the averaged test statistic T_k as defined in Theorem 3 for detecting shifts for all $n = 28$ brain regions by Algorithm 2, with a focus on identifying regions where ADHD patients deviate the most from controls. For each brain region, the blue bar represents the test statistic T_k obtained by comparing the brain networks of each ADHD patient with each control across all combinations, with the final value being the average of these T_k values, and the lighter-colored bar represent T_k obtained by comparing brain networks within the control group, considering all possible pairs, with the final value being the average of these T_k values.

From Figure 8, we can see that the averaged test statistics T_k between controls, computed for all brain regions, are generally on the same scale and are almost always smaller than the critical value for detecting shifts, as specified in Theorem 3 and represented by

the horizontal red dashed line in Figure 8. The averaged T_k across patients and controls for all brain regions are typically larger than those between controls alone. Brain regions with larger differences in these T_k values are likely to be more significant for understanding ADHD. Notably, the differences in the leftmost 7 brain regions in Figure 8 are larger than those in other regions and significantly exceed the critical value. In addition, the regions SWAG and SMAD also exhibit T_k values across patients and controls that are notably greater than the critical value. Finally, these brain regions – F1OD, F2OG, F3OG, F2OD, SMAG, GRG, SMAD, F1OG, GRD, and ORD – are likely to be important for understanding ADHD.

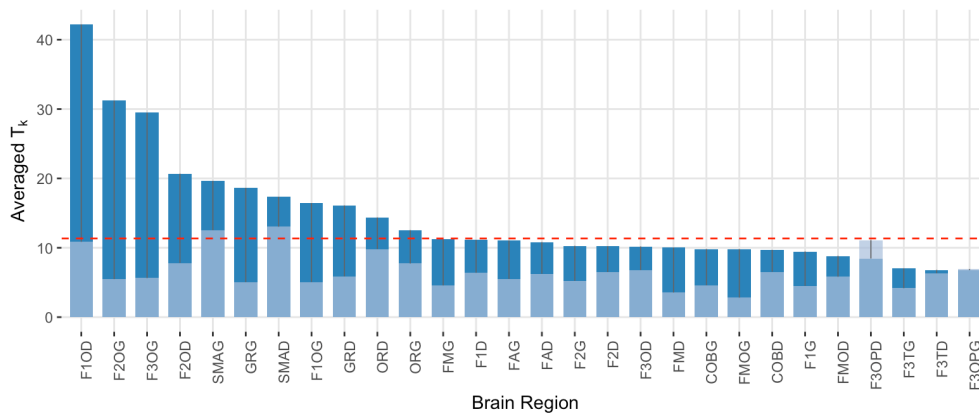


Figure 8: Comparison of brain region latent position shifts between ADHD patients and controls, and within controls using Algorithm 2. The blue bars represent the average test statistic T_k (as defined in Theorem 3) by comparing the brain networks across patients and controls. The lighter-colored bars represent the average T_k by comparing brain networks within the control group. The horizontal red dashed line represents the critical value for detecting shifts, as specified in Theorem 3.

6.2 Dynamic chocolate trading network

We consider the dynamic trading network between countries for chocolate during the year from 2010 to 2022. The data is collected by the Food and Agriculture Organization of the United Nations and is available at <https://www.fao.org/faostat/en/#data/TM>. We construct a dynamic trading network of chocolate for $T = 2022 - 2020 + 1 = 13$ time points,

where vertices represent countries and edges in each network represent trade relationships between countries. For each time point t , we obtain the adjacency matrix $\mathbf{A}^{(t)}$ by (1) we set $(\mathbf{A}^{(t)})_{r,s} = (\mathbf{A}^{(t)})_{s,r} = 1$ if there is trade between countries r and s ; (2) we ignore the links between countries r and s in $\mathbf{A}^{(t)}$ if their total trade amount at the time point t is less than two hundred thousands US dollars; (3) finally we extract the intersection of the largest connected components of $\{\mathbf{A}^{(t)}\}$ to get the networks for the common involved countries. The resulting adjacency matrices $\{\mathbf{A}^{(t)}\}_{t \in [T]}$ corresponding to $T = 13$ time points on a set of $n = 169$ vertices.

We now consider the first year, 2010, and the last year, 2022, to compare the trading networks $\mathbf{A}^{(1)}$ and $\mathbf{A}^{(13)}$, estimating the sets of countries with unshifted embeddings and shifted embeddings, \mathcal{U} and \mathcal{U}^c , as well as the shifts \mathbf{Y} by Algorithm 2. We set the embedding dimension to $d = 2$, the significance level for detecting shifts to $\alpha = 0.01$, and the other parameters of Algorithm 2 to $L = 3$, $M = 5000$, and $\tau = 0.3$. We identify $|\hat{\mathcal{U}}| = 148$ countries with unshifted embeddings $\hat{\mathcal{U}}$, leaving 21 countries with shifted embeddings $\hat{\mathcal{U}}^c$. Figure 9 shows the test statistics T_k for all countries. In Figure 9, countries with significant T_k values often align with real-world changes in chocolate trade over the past decade. For instance, Poland, which has a high T_k , is a major chocolate producer and exporter in Europe with growing export volumes. Similarly, China has experienced a significant surge in chocolate consumption and imports over the past decade, which explains its significant T_k . Figure 10 shows the proportions of countries with unshifted and shifted embeddings across different regions. It can be observed that a higher proportion of Asian and European countries experience shifts in their embeddings for chocolate trade between these two time points. Figure 11 provides the estimates of embedding changes for countries with shifted embeddings, i.e., rows of $\hat{\mathbf{Y}}_{\hat{\mathcal{U}}^c}$. Figure 11 shows that countries on the same continent are generally placed close together, indicating a strong correlation between the estimated embedding shifts and the true underlying geographic proximities. Here, we just compare

the networks for two specific time points, while in Section 7.1 we will extend the analysis to the entire dynamic chocolate trading network by considering all pairs of time points.

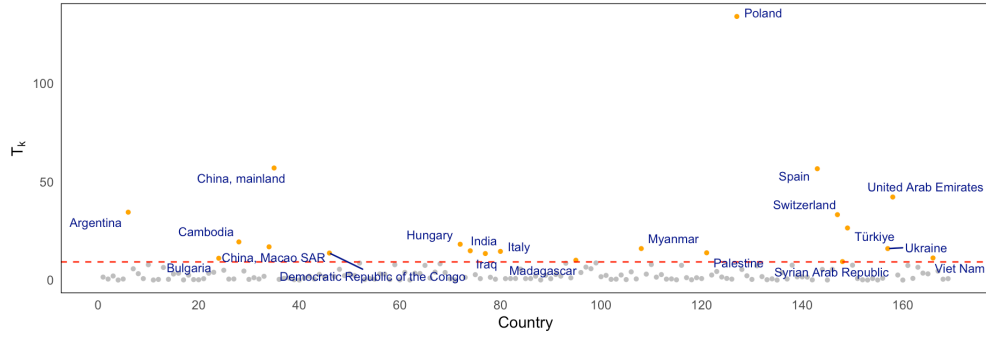


Figure 9: The test statistics $\{T_k\}_{k \in [n]}$ for all $n = 169$ countries. The red horizontal dashed line indicates the critical value $c_{\alpha=0.01}$, used to reject the null hypothesis that there is no shift for a given country. The countries with shifted embeddings are labeled by their names.

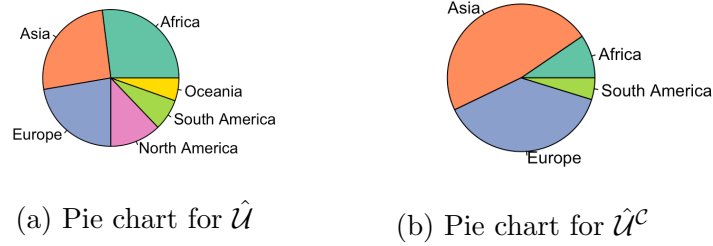


Figure 10: Proportions of countries with unshifted and shifted embeddings.

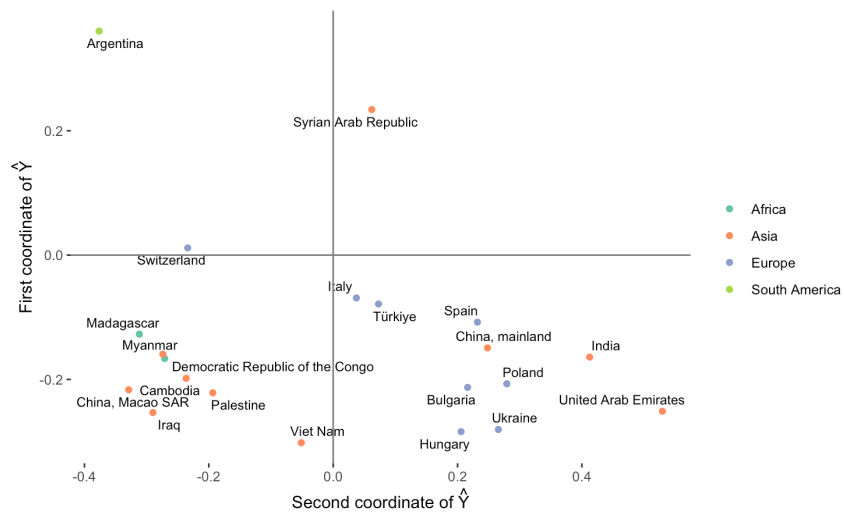


Figure 11: Embedding shifts for countries in \hat{U}^c , corresponding to the rows of $\hat{Y}_{\hat{U}^c}$.

7 Extensions

7.1 Related Euclidean mirrors for dynamic networks

For a dynamic network, [Athreya et al. \[2024\]](#) propose the idea of *mirror* to visualize the network evolution pattern with a curve in low-dimensional Euclidean space. More specifically, for a dynamic network $\{\mathbf{A}^{(i)}\}_{i \in [T]}$, where T is the number of time points and $\mathbf{A}^{(t)}$ is the adjacency matrix of the network at time point t , we measure the difference $\hat{\mathbf{D}}_{i,j}$ between each pair of networks $(\mathbf{A}^{(i)}, \mathbf{A}^{(j)})$ for all observed time points $i, j \in [T]$, and then classical multidimensional scaling (CMDS) [[Borg and Groenen, 2007](#), [Li et al., 2020](#), [Wickelmaier, 2003](#)] is applied to obtain a configuration in a low-dimensional space that approximately preserves the dissimilarity in $\hat{\mathbf{D}} \in \mathbb{R}^{T \times T}$. This results in a curve whose coordinates are the rows of $\hat{\mathbf{M}} \in \mathbb{R}^{T \times r}$ in r -dimensional Euclidean space, representing the evolution of the network dynamics over the T time points, referred to as the mirror of the dynamic network. After the mirror is obtained, using the ISOMAP technique [[Tenenbaum et al., 2000](#)], the mirror in r -dimensional space can be further reduced to a 1-dimensional curve, called the *iso-mirror*, where the Euclidean distances approximate the geodesic distances along the mirror, and thus larger changes along the y-axis of the iso-mirror correspond to significant changes in the network.

In the initial mirror algorithm proposed by [Athreya et al. \[2024\]](#), the difference $\hat{\mathbf{D}}_{i,j}$ between each pair of networks $(\mathbf{A}^{(i)}, \mathbf{A}^{(j)})$ is defined as

$$\hat{\mathbf{D}}_{i,j} = \min_{\mathbf{O} \in \mathcal{O}_d} \|\hat{\mathbf{X}}^{(i)} \mathbf{O} - \hat{\mathbf{X}}^{(j)}\| / \sqrt{n},$$

which estimates the pairwise distance between the two estimated latent position matrices $\hat{\mathbf{X}}^{(i)}, \hat{\mathbf{X}}^{(j)} \in \mathbb{R}^{n \times d}$. In this paper, under the model where the latent positions of some vertices remain unchanged while others are shifted, the distance between two networks can alternatively be defined, such as by the proportion of shifted vertices, given by

$$\hat{\mathbf{D}}_{i,j} = |(\hat{\mathcal{U}}^{(i,j)})^c| / n, \tag{5}$$

where $(\hat{\mathcal{U}}^{(i,j)})^c$ denotes the set of shifted vertices between networks i and j , and can be obtained by Algorithm 2.

We now consider the entire dynamic trading network $\{\mathbf{A}^{(t)}\}_{t \in [13]}$ for chocolate trading, as described in Section 6.2, and construct its mirror to approximately preserve the distances defined in Eq. (5) with the embedding dimension r set to 2. The mirror and corresponding iso-mirror are shown in Figure 12, and they show that there are more countries with changes in global chocolate trading patterns between 2010 and 2011, and between 2020 and 2021.

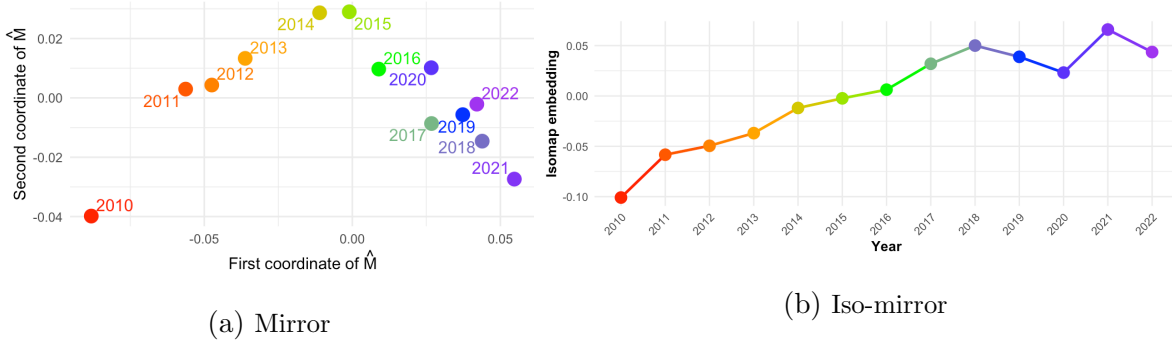


Figure 12: Mirror and iso-mirror for the entire chocolate dynamic trading network.

The above idea focuses on constructing a low-dimensional mirror to represent the evolution pattern of the *entire* dynamic network. Similarly, we can also focus on *a specific vertex* and construct a mirror to describe the changes in its latent position over time. For a specific vertex $k \in [n]$, we define the distance between each pair of time points (i, j) as

$$\hat{\mathbf{D}}_{i,j}^{[k]} = \begin{cases} 0 & \text{if } k \in \hat{\mathcal{U}}^{(i,j)}, \\ \|\hat{\mathbf{y}}_k\| & \text{if } k \in (\hat{\mathcal{U}}^{(i,j)})^c. \end{cases} \quad (6)$$

This means that if vertex k is estimated to be unshifted between time points i and j , the distance is defined as 0, and if vertex k is estimated to be shifted, the distance is defined as the norm of its estimated shift $\hat{\mathbf{y}}_k$.

Using the distance defined in Eq. (6), we generate the mirror and corresponding iso-mirror for Poland as a vertex in the dynamic chocolate trading network, as shown in Fig-

ure 13. Figure 13 indicates that Poland’s chocolate trading pattern experienced significant changes before 2016 and became relatively stable thereafter.

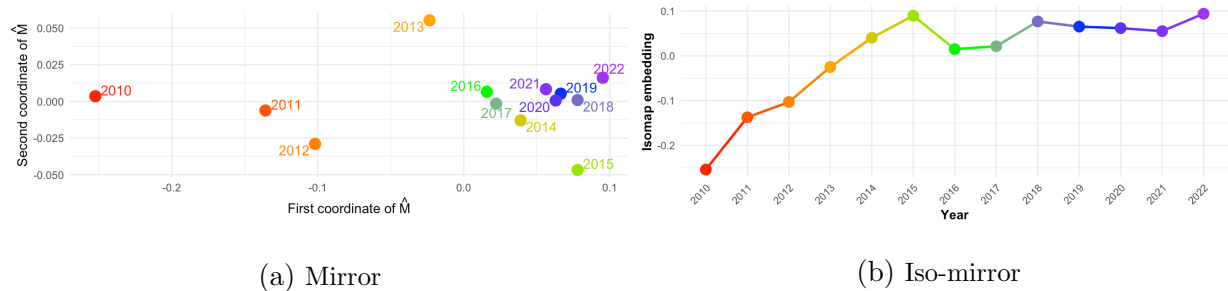


Figure 13: Mirror and iso-mirror for Poland in the chocolate dynamic trading network.

7.2 Extension to generalized random dot product graphs (GRDPGs)

We extend the model to pairs of random networks based on the GRDPG model [Rubin-Delanchy et al., 2017, Young and Scheinerman, 2007], which generalizes the RDPG model by allowing for indefinite inner products.

Definition 2 (Generalized random dot product graph (GRDPG)). *Let $d \geq 1$ be given and let \mathcal{X} be a subset of \mathbb{R}^d such that $x^\top \mathbf{I}_{d_+, d_-} y \in [0, 1]$ for any $x, y \in \mathcal{X}$. Here, \mathbf{I}_{d_+, d_-} is a $d \times d$ diagonal matrix with d_+ diagonal entries equal to $+1$ and d_- diagonal entries equal to -1 , where d_+ and d_- are non-negative integers satisfying $d_+ + d_- = d$. For a given $n \geq 1$, let $\mathbf{X} = [\mathbf{x}_1, \mathbf{x}_2, \dots, \mathbf{x}_n]^\top$ be a $n \times d$ matrix with $\mathbf{x}_k \in \mathcal{X}$ for all $k \in [n]$. A random network G is said to be a generalized random dot product graph with latent positions of the vertices in \mathbf{X} , where each row $\mathbf{x}_k \in \mathbb{R}^d$ denotes the latent position for the k th vertex, if the adjacency matrix \mathbf{A} of G is a symmetric matrix whose upper triangular entries $\{\mathbf{A}_{s,t}\}_{s < t}$ are independent Bernoulli random variables with*

$$\mathbf{A}_{s,t} \sim \text{Bernoulli}(\mathbf{x}_s^\top \mathbf{I}_{d_+, d_-} \mathbf{x}_t).$$

We define $\mathbf{P} := \mathbf{X} \mathbf{I}_{d_+, d_-} \mathbf{X}^\top$ as the connection probability matrix of G and denote such a graph by $\text{GRDPG}(\mathbf{X} \mathbf{I}_{d_+, d_-} \mathbf{X}^\top)$. In this case, the success probabilities of $\{\mathbf{A}_{s,t}\}_{s < t}$ are given

by $\mathbf{P}_{s,t} = \mathbf{x}_s^\top \mathbf{I}_{d_+,d_-} \mathbf{x}_t$.

Remark 6 (Indefinite orthogonal nonidentifiability in GRDPGs). *Note that if $G \sim \text{GRDPG}(\mathbf{X}\mathbf{I}_{d_+,d_-}\mathbf{X}^\top)$ with the latent position matrix $\mathbf{X} \in \mathbb{R}^{n \times d}$, then for any orthogonal matrix $\mathbf{W} \in \mathcal{O}_{d_+,d_-}$, $\mathbf{X}\mathbf{W}$ also gives rise to a GRDPG with the same probability distribution. Here $\mathcal{O}_{d_+,d_-} := \{\mathbf{O} \in \mathbb{R}^{d \times d} \mid \mathbf{O}\mathbf{I}_{d_+,d_-}\mathbf{O}^\top = \mathbf{I}_{d_+,d_-}\}$ is the indefinite orthogonal group.*

Assume that $G^{(1)}$ and $G^{(2)}$ are independent GRDPGs with latent position matrices $\mathbf{X}^{(1)}$ and $\mathbf{X}^{(2)}$, respectively, i.e., $G^{(i)} \sim \text{GRDPG}(\mathbf{X}^{(i)}\mathbf{I}_{d_+,d_-}\mathbf{X}^{(i)\top})$ for $i \in \{1, 2\}$. For the set of unshifted vertices $\mathcal{U} \subseteq [n]$, there exists an indefinite orthogonal matrix $\mathbf{W}^{(1,2)} \in \mathcal{O}_{d_+,d_-}$ such that $\mathbf{X}_{\mathcal{U}}^{(2)} = \mathbf{X}_{\mathcal{U}}^{(1)}\mathbf{W}^{(1,2)}$. And for the latent position matrix $\mathbf{Y} \in \mathbb{R}^{n \times d}$ with $\mathbf{Y}_{\mathcal{U}} = \mathbf{0}$, we have $\mathbf{X}^{(2)} = \mathbf{X}^{(1)}\mathbf{W}^{(1,2)} + \mathbf{Y}$.

Given each observed adjacency matrix $\mathbf{A}^{(i)}$ of the GRDPG, the estimated latent position matrix is computed as $\hat{\mathbf{X}}^{(i)} = \hat{\mathbf{U}}^{(i)}|\hat{\mathbf{\Lambda}}^{(i)}|^{1/2}$, where $\hat{\mathbf{\Lambda}}^{(i)} = \text{diag}(\hat{\mathbf{\Lambda}}_+^{(i)}, \hat{\mathbf{\Lambda}}_-^{(i)})$ is a $d \times d$ diagonal matrix, and $\hat{\mathbf{\Lambda}}_+^{(i)}$ and $\hat{\mathbf{\Lambda}}_-^{(i)}$ contain the d_+ largest positive and d_- largest (in magnitude) negative eigenvalues of $\mathbf{A}^{(i)}$, respectively. $\hat{\mathbf{U}}^{(i)} = [\hat{\mathbf{U}}_+^{(i)}, \hat{\mathbf{U}}_-^{(i)}]$ contains the corresponding eigenvectors.

In this case, for a given seed set $\mathcal{S} \subset \mathcal{U}$ with $|\mathcal{S}| \geq d$, we aim to obtain $\hat{\mathbf{W}}^{(1,2)}$ by solving the indefinite orthogonal Procrustes problem

$$\hat{\mathbf{W}}^{(1,2)} = \arg \min_{\mathbf{O} \in \mathcal{O}_{d_+,d_-}} \|\hat{\mathbf{X}}_{\mathcal{S}}^{(1)}\mathbf{O} - \hat{\mathbf{X}}_{\mathcal{S}}^{(2)}\|_F = \arg \min_{\mathbf{O} \in \mathcal{O}_{d_+,d_-}} \|\hat{\mathbf{X}}_{\mathcal{S}}^{(1)}\mathbf{I}_{d_+,d_-} - \hat{\mathbf{X}}_{\mathcal{S}}^{(2)}\mathbf{I}_{d_+,d_-}\mathbf{O}^\top\|_F,$$

but there is no longer an analytical solution due to the indefinite orthogonality constraint, so we approximate the solution by relaxing the problem into two unconstrained least squares problems

$$\hat{\mathbf{W}}_L^{(1,2)} = \underset{\mathbf{O} \in \mathbb{R}^{d \times d}}{\text{argmin}} \|\hat{\mathbf{X}}_{\mathcal{S}}^{(1)}\mathbf{O} - \hat{\mathbf{X}}_{\mathcal{S}}^{(2)}\|_F, \quad (7)$$

$$\hat{\mathbf{W}}_R^{(1,2)} = \underset{\mathbf{O} \in \mathbb{R}^{d \times d}}{\text{argmin}} \|\hat{\mathbf{X}}_{\mathcal{S}}^{(1)}\mathbf{I}_{d_+,d_-} - \hat{\mathbf{X}}_{\mathcal{S}}^{(2)}\mathbf{I}_{d_+,d_-}\mathbf{O}^\top\|_F, \quad (8)$$

The solution to Eq. (7) is given by $\hat{\mathbf{W}}_L^{(1,2)} = (\mathbf{X}_{\mathcal{S}}^{(1)\top}\mathbf{X}_{\mathcal{S}}^{(1)})^{-1}\mathbf{X}_{\mathcal{S}}^{(1)\top}\mathbf{X}_{\mathcal{S}}^{(2)} = (\mathbf{X}_{\mathcal{S}}^{(1)})^\dagger\mathbf{X}_{\mathcal{S}}^{(2)}$, where $(\cdot)^\dagger$ denotes the Moore-Penrose pseudoinverse. Similarly, the solution to Eq. (8) is $\hat{\mathbf{W}}_R^{(1,2)} =$

$[(\hat{\mathbf{X}}_S^{(2)} \mathbf{I}_{d_+, d_-})^\dagger \hat{\mathbf{X}}_S^{(1)} \mathbf{I}_{d_+, d_-}]^\top$. We combine the two solutions by setting $\hat{\mathbf{W}}^{(1,2)} = \frac{1}{2}(\hat{\mathbf{W}}_L^{(1,2)} + \hat{\mathbf{W}}_R^{(1,2)})$, and subsequently compute the estimated shift matrix as $\hat{\mathbf{Y}} = \hat{\mathbf{X}}^{(2)} - \hat{\mathbf{X}}^{(1)} \hat{\mathbf{W}}^{(1,2)}$. Based on Theorem 3.2 of Xie [2024] and the analysis in Lemma D.13 of Zheng and Tang [2024], we can derive the test statistic T_k with an almost identical formula as in Eq. (4) with the only difference being the definition of the estimated covariance matrix, which is given by

$$\begin{aligned} \hat{\mathbf{\Gamma}}^{(k)} := & \mathbf{I}_{d_+, d_-} (\hat{\mathbf{X}}^{(2)\top} \hat{\mathbf{X}}^{(2)})^{-1} \hat{\mathbf{X}}^{(2)\top} \hat{\mathbf{\Xi}}^{(k,2)} \hat{\mathbf{X}}^{(2)} (\hat{\mathbf{X}}^{(2)\top} \hat{\mathbf{X}}^{(2)})^{-1} \mathbf{I}_{d_+, d_-} \\ & + \hat{\mathbf{W}}^{(1,2)\top} \mathbf{I}_{d_+, d_-} (\hat{\mathbf{X}}^{(1)\top} \hat{\mathbf{X}}^{(1)})^{-1} \hat{\mathbf{X}}^{(1)\top} \hat{\mathbf{\Xi}}^{(k,1)} \hat{\mathbf{X}}^{(1)} (\hat{\mathbf{X}}^{(1)\top} \hat{\mathbf{X}}^{(1)})^{-1} \mathbf{I}_{d_+, d_-} \hat{\mathbf{W}}^{(1,2)}. \end{aligned}$$

With the above test statistic T_k , we have the corresponding Algorithm 1 and Algorithm 2 for the GRDPG framework.

We explore the performance of the corresponding Algorithm 2 in the no-seed scenario under the GRDPG framework. Consider the setting of Section 5.4, but with the block-wise probability matrix

$$\mathbf{B} = \begin{bmatrix} 0.7 & 0.1 & 0.1 \\ 0.1 & 0.3 & 0.8 \\ 0.1 & 0.8 & 0.5 \end{bmatrix},$$

and thus $d_+ = 2, d_- = 1$. Figure 14 presents the accuracy results and running time of the algorithm, and it demonstrate that the algorithm achieves high accuracy in identifying unshifted vertices while maintaining computational efficiency.

8 Discussion

We now mention several potential directions for future research. Firstly, in this paper we focus on the setting where the unshifted vertices between the two networks share the same latent positions (up to an orthogonal transformation), i.e., $\mathbf{X}_u^{(2)} = \mathbf{X}_u^{(1)} \mathbf{W}^{(1,2)}$. A natural extension would be to consider more general scenarios where the latent positions of the unshifted vertices undergo scaling or diagonal transformations. Such flexible settings

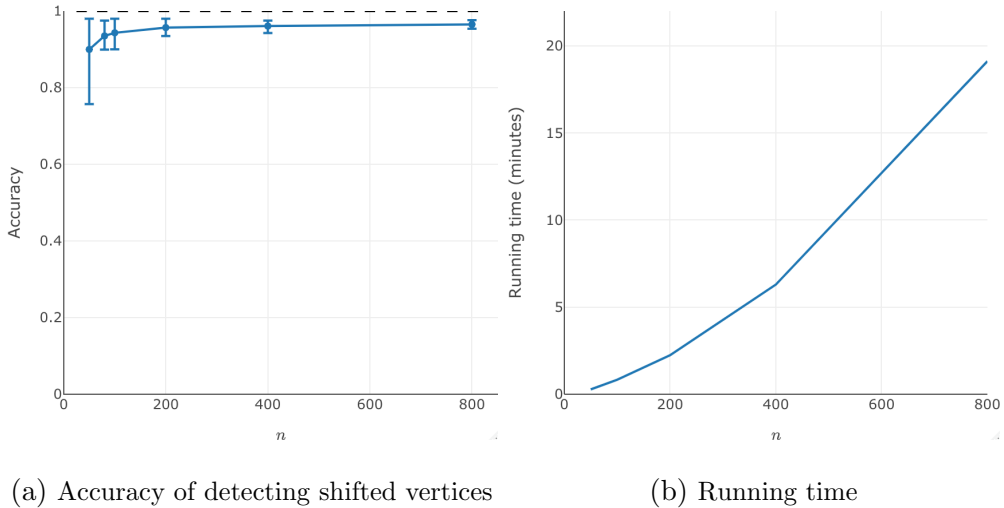


Figure 14: Panel (a) illustrates the accuracy of detecting shifted vertices without seeds, as we vary the number of vertices $n \in \{50, 80, 100, 200, 400, 800\}$ while setting $L = 3$, $M = 1000$, $\alpha = 0.05$, $\tau = 0.3$. Panel (a) reports the mean, along with the 0.05 and 0.95-quantile points, based on 100 independent Monte Carlo replicates of two SBMs on n vertices with $d = 3$ blocks consisting of $d_+ = 2$ positive and $d_- = 1$ negative eigenvalues, where the block assignments of half of the vertices are shifted. Panel (b) reports the running time on a standard computer for 100 Monte Carlo replicates.

have been explored in the context of other two-sample network inference problems in the existing literature [Du and Tang, 2023, Tang et al., 2017a,b]. Our framework can also be extended to address the shift detection and estimation problem under these generalized models, such as considering $\mathbf{X}_{\mathcal{U}}^{(2)} = c_n \mathbf{X}_{\mathcal{U}}^{(1)} \mathbf{W}^{(1,2)}$ for some scaling factor c_n depending on n , or $\mathbf{X}_{\mathcal{U}}^{(2)} = \mathbf{D}_n \mathbf{X}_{\mathcal{U}}^{(1)} \mathbf{W}^{(1,2)}$ for some diagonal \mathbf{D}_n .

Secondly, our current model focuses on undirected networks, which can be extended to directed networks [Leicht and Newman, 2008, Malliaros and Vazirgiannis, 2013] by assuming $\mathbf{P}^{(i)} = \mathbf{X}^{(i)} \mathbf{Y}^{(i)\top}$, where $\mathbf{X}^{(i)}$ represents the latent positions of the source vertices and $\mathbf{Y}^{(i)}$ represents the latent positions of the target vertices in network i . Denoting the set of unshifted source vertices by \mathcal{U} and the set of unshifted target vertices by \mathcal{V} , our method can be extended to identify the sets \mathcal{U} and \mathcal{V} and estimate the corresponding shifts.

Finally, the concept of detecting latent position shifts can be extended beyond networks to various latent position models in machine learning applications. For instance, latent

factor models, such as matrix factorization [He et al., 2016, Ma et al., 2008], extract latent features from user-item interaction data and are widely used in recommendation systems, and detecting shifts in these latent representations can provide insights into evolving user preferences and changes in item popularity over time.

References

- Emmanuel Abbe, Jianqing Fan, Kaizheng Wang, and Yiqiao Zhong. Entrywise eigenvector analysis of random matrices with low expected rank. *Annals of Statistics*, 48(3):1452–1474, 2020.
- S. C. Ahn and A. R. Horenstein. Eigenvalue ratio test for the number of factors. *Econometrica*, 81:1203–1227, 2013.
- Avanti Athreya, Donniell E Fishkind, Minh Tang, Carey E Priebe, Youngser Park, Joshua T Vogelstein, Keith Levin, Vince Lyzinski, Yichen Qin, and Daniel L Sussman. Statistical inference on random dot product graphs: a survey. *Journal of Machine Learning Research*, 18:1–92, 2018.
- Avanti Athreya, Zachary Lubberts, Youngser Park, and Carey Priebe. Euclidean mirrors and dynamics in network time series. *Journal of the American Statistical Association*, (just-accepted):1–41, 2024.
- Ingwer Borg and Patrick JF Groenen. *Modern multidimensional scaling: Theory and applications*. Springer Science & Business Media, 2007.
- Changxiao Cai, Gen Li, Yuejie Chi, H Vincent Poor, and Yuxin Chen. Subspace estimation from unbalanced and incomplete data matrices: $\ell_{2,\infty}$ statistical guarantees. *Annals of Statistics*, 49:944–967, 2021.

- E. J. Candes and B. Recht. Exact matrix completion via convex optimization. *Foundations of Computational Mathematics*, 9:717–772, 2009.
- Joshua Cape, Minh Tang, and Carey E Priebe. The two-to-infinity norm and singular subspace geometry with applications to high-dimensional statistics. *Annals of Statistics*, 47(5):2405–2439, 2019.
- Yuxin Chen, Yuejie Chi, Jianqing Fan, and Cong Ma. Spectral methods for data science: a statistical perspective. *Foundations and Trends® in Machine Learning*, 14(5):566–806, 2021.
- ADHD-200 consortium. The adhd-200 consortium: a model to advance the translational potential of neuroimaging in clinical neuroscience. *Frontiers in systems neuroscience*, 6:62, 2012.
- A. Damle and Y. Sun. Uniform bounds for invariant subspace perturbations. *SIAM Journal on Matrix Analysis and Applications*, 41(3):1208–1236, 2020.
- P. Diaconis and S. Janson. Graph limits and exchangeable random graphs. *Rendiconti di Matematica, Serie VII*, 28:33–61, 2008.
- Xinjie Du and Minh Tang. Hypothesis testing for equality of latent positions in random graphs. *Bernoulli*, 29(4):3221–3254, 2023.
- Jianqing Fan, Weichen Wang, and Yiqiao Zhong. An ℓ_∞ eigenvector perturbation bound and its application to robust covariance estimation. *Journal of Machine Learning Research*, 18(207):1–42, 2018.
- Debarghya Ghoshdastidar, Maurilio Gutzeit, Alexandra Carpentier, and Ulrike von Luxburg. Two-sample tests for large random graphs using network statistics. In *Conference on Learning Theory*, pages 954–977. PMLR, 2017.

- Debarghya Ghoshdastidar, Maurilio Gutzeit, Alexandra Carpentier, and Ulrike Von Luxburg. Two-sample hypothesis testing for inhomogeneous random graphs. *The Annals of Statistics*, 48(4):2208–2229, 2020.
- Zeus Gracia-Tabuenca and Sarael Alcauter. Nbr: network-based r-statistics for (unbalanced) longitudinal samples. *bioRxiv*, 2020. URL <https://doi.org/10.1101/2020.11.07.373019>.
- Xiao Han, Qing Yang, and Yingying Fan. Universal rank inference via residual subsampling with application to large networks. *Annals of Statistics*, 51:1109–1133, 2023.
- Xiangnan He, Hanwang Zhang, Min-Yen Kan, and Tat-Seng Chua. Fast matrix factorization for online recommendation with implicit feedback. In *Proceedings of the 39th International ACM SIGIR conference on Research and Development in Information Retrieval*, pages 549–558, 2016.
- P. D. Hoff, A. E. Raftery, and M. S. Handcock. Latent space approaches to social network analysis. *Journal of the American Statistical Association*, 97(460):1090–1098, 2002.
- Paul W Holland, Kathryn Blackmond Laskey, and Samuel Leinhardt. Stochastic block-models: First steps. *Social networks*, 5(2):109–137, 1983.
- S. Van Huffel. Partial singular value decomposition algorithm. *Journal of computational and applied mathematics*, 33(1):105–112, 1990.
- Jiashun Jin, Zheng Tracy Ke, Shengming Luo, and Yucong Ma. Optimal network pairwise comparison. *Journal of the American Statistical Association*, (just-accepted):1–25, 2024.
- Lihua Lei. Unified $\ell_{2 \rightarrow \infty}$ eigenspace perturbation theory for symmetric random matrices. arXiv preprint at <https://arxiv.org/abs/1909.04798>, 2019.
- Elizabeth A Leicht and Mark EJ Newman. Community structure in directed networks. *Physical review letters*, 100(11):118703, 2008.

- Gongkai Li, Minh Tang, Nicolas Charon, and Carey Priebe. Central limit theorems for classical multidimensional scaling. *Electronic Journal of Statistics*, 14(1):2362–2394, 2020.
- Ren-Cang Li. New perturbation bounds for the unitary polary factor. *SIAM Journal on Matrix Analysis and its Applications*, 16:327–332, 1995.
- Yezheng Li and Hongzhe Li. Two-sample test of community memberships of weighted stochastic block models. *arXiv preprint arXiv:1811.12593*, 2018.
- Fuchen Liu, David Choi, Lu Xie, and Kathryn Roeder. Global spectral clustering in dynamic networks. *Proceedings of the National Academy of Sciences*, 115(5):927–932, 2018.
- L. Lovász. *Large networks and graph limits*. American Mathematical Society, 2012.
- Hao Ma, Haixuan Yang, Michael R Lyu, and Irwin King. Sorec: social recommendation using probabilistic matrix factorization. In *Proceedings of the 17th ACM conference on Information and knowledge management*, pages 931–940, 2008.
- Fragkiskos D Malliaros and Michalis Vazirgiannis. Clustering and community detection in directed networks: A survey. *Physics reports*, 533(4):95–142, 2013.
- Maarten Mennes, Bharat B Biswal, F Xavier Castellanos, and Michael P Milham. Making data sharing work: the fcp/indi experience. *Neuroimage*, 82:683–691, 2013.
- A. Onatski. Determining the number of factors from empirical distribution of eigenvalues. *Review of Economics and Statistics*, 92:1004–1016, 2010.
- Guilherme Polanczyk, Maurício Silva De Lima, Bernardo Lessa Horta, Joseph Biederman, and Luis Augusto Rohde. The worldwide prevalence of adhd: a systematic review and metaregression analysis. *American journal of psychiatry*, 164(6):942–948, 2007.
- P. Rubin-Delanchy, C. E. Priebe, M. Tang, and J. Cape. A statistical interpretation of

- spectral embedding: the generalised random dot product graph. arXiv preprint at <http://arxiv.org/abs/1709.05506>, 2017.
- Åsa Segerstolpe, Athanasia Palasantza, Pernilla Eliasson, Eva-Marie Andersson, Anne-Christine Andréasson, Xiaoyan Sun, Simone Picelli, Alan Sabirsh, Maryam Clausen, Magnus K Bjursell, et al. Single-cell transcriptome profiling of human pancreatic islets in health and type 2 diabetes. *Cell metabolism*, 24(4):593–607, 2016.
- Minh Tang, Avanti Athreya, Daniel L Sussman, Vince Lyzinski, Youngser Park, and Carey E Priebe. A semiparametric two-sample hypothesis testing problem for random graphs. *Journal of Computational and Graphical Statistics*, 26(2):344–354, 2017a.
- Minh Tang, Avanti Athreya, Daniel L Sussman, Vince Lyzinski, and Carey E Priebe. A nonparametric two-sample hypothesis testing problem for random graphs. *Bernoulli*, 23(3):1599–1630, 2017b.
- Joshua B Tenenbaum, Vin de Silva, and John C Langford. A global geometric framework for nonlinear dimensionality reduction. *science*, 290(5500):2319–2323, 2000.
- Aad W Van der Vaart. *Asymptotic statistics*. Cambridge University Press, 2000.
- Bernadette CM Van Wijk, Cornelis J Stam, and Andreas Daffertshofer. Comparing brain networks of different size and connectivity density using graph theory. *PloS one*, 5(10):e13701, 2010.
- Florian Wickelmaier. An introduction to mds. *Sound Quality Research Unit, Aalborg University, Denmark*, 46:1–26, 2003.
- Fangzheng Xie. Entrywise limit theorems for eigenvectors of signal-plus-noise matrix models with weak signals. *Bernoulli*, 30(1):388–418, 2024.

- S. J. Young and E. R. Scheinerman. Random dot product graph models for social networks. In *International Workshop on Algorithms and Models for the Web-Graph*, pages 138–149. Springer, 2007.
- Andrew Zalesky, Alex Fornito, and Edward T Bullmore. Network-based statistic: identifying differences in brain networks. *Neuroimage*, 53(4):1197–1207, 2010.
- Runbing Zheng and Minh Tang. Limit results for distributed estimation of invariant subspaces in multiple networks inference and pca. *arXiv preprint arXiv:2206.04306*, 2022.
- Runbing Zheng and Minh Tang. Chain-linked multiple matrix integration via embedding alignment. *arXiv preprint arXiv:2412.02791*, 2024.
- Mu Zhu and Ali Ghodsi. Automatic dimensionality selection from the scree plot via the use of profile likelihood. *Computational Statistics & Data Analysis*, 51(2):918–930, 2006.

A Additional Experiment Results

A.1 Additional simulation results

In Section 5.1, we present the error results for an unshifted vertex ($k = 1$) for the simulation experiment. Here, we further present the estimation error results for a shifted vertex ($k = 1001$) in Figure A.1 and Figure A.2. Henze-Zirkler’s normality test indicates that the empirical distribution of $\mathbf{W}^\top \hat{\mathbf{y}}_k - \mathbf{y}_k$ for $k = 1001$ is well-approximated by a multivariate normal distribution, and Figure A.1 and Figure A.2 illustrate that the empirical distribution closely matches the theoretical distribution provided in Theorem 2.

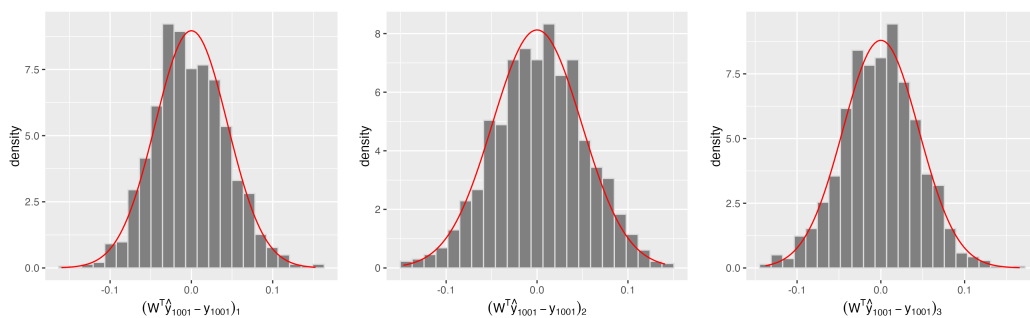


Figure A.1: Histograms of the empirical distributions of the entries of the estimation error $\mathbf{W}^\top \hat{\mathbf{y}}_k - \mathbf{y}_k$ for $k = 1001$. These histograms are based on 1000 independent Monte Carlo replicates of two RDPGs on $n = 2000$ vertices with $d = 3$ dimensional latent positions, where half of the vertices are shifted. The red lines represent the probability density functions of the normal distributions with parameters specified in Theorem 2.

A.2 Additional results for the contrastive study of brain networks in ADHD

We now present additional results and analysis to complement Section 6.1. From Figure A.3, we observe that within the control group, the test statistic T_k for all brain regions are generally smaller than the critical value for detecting shifts. This indicates that there are no significant shifts in any brain regions between controls. Furthermore, Figure A.3

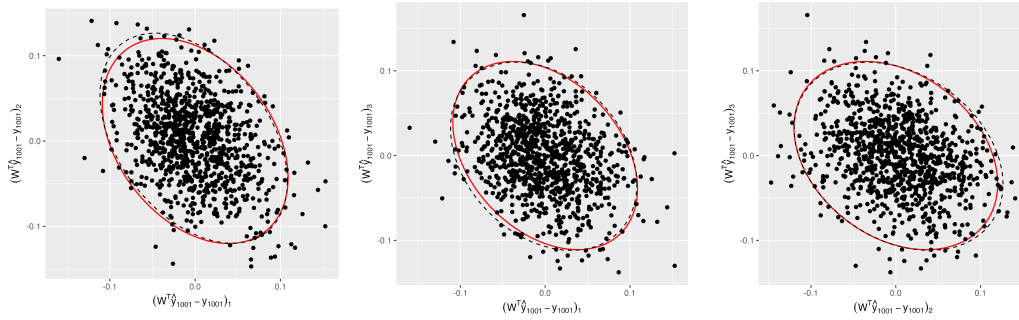


Figure A.2: Bivariate plots for the empirical distributions between the entries of the estimation error $\mathbf{W}^\top \hat{\mathbf{y}}_k - \mathbf{y}_k$ for $k = 1001$ based on 1000 Monte Carlo replicates of the same setting with Figure 3. Dashed black ellipses represent 95% level curves for the empirical distributions while solid red ellipses represent 95% level curves for the theoretical distributions as specified in Theorem 2.

shows that the number of brain regions with shifts is considerably large between patients and controls, as well as within patients.

In Section 6.1, we concluded that the brain regions – F1OD, F2OG, F3OG, F2OD, SMAG, GRG, SMAD, F1OG, GRD, and ORD – are likely to be important for understanding ADHD. Among these regions, some, such as F1OG, F2OG, and F3OG, exhibit relatively small T_k values within patients. This indicates a high degree of similarity in these brain regions among patients, suggesting that they warrant further focused investigation.

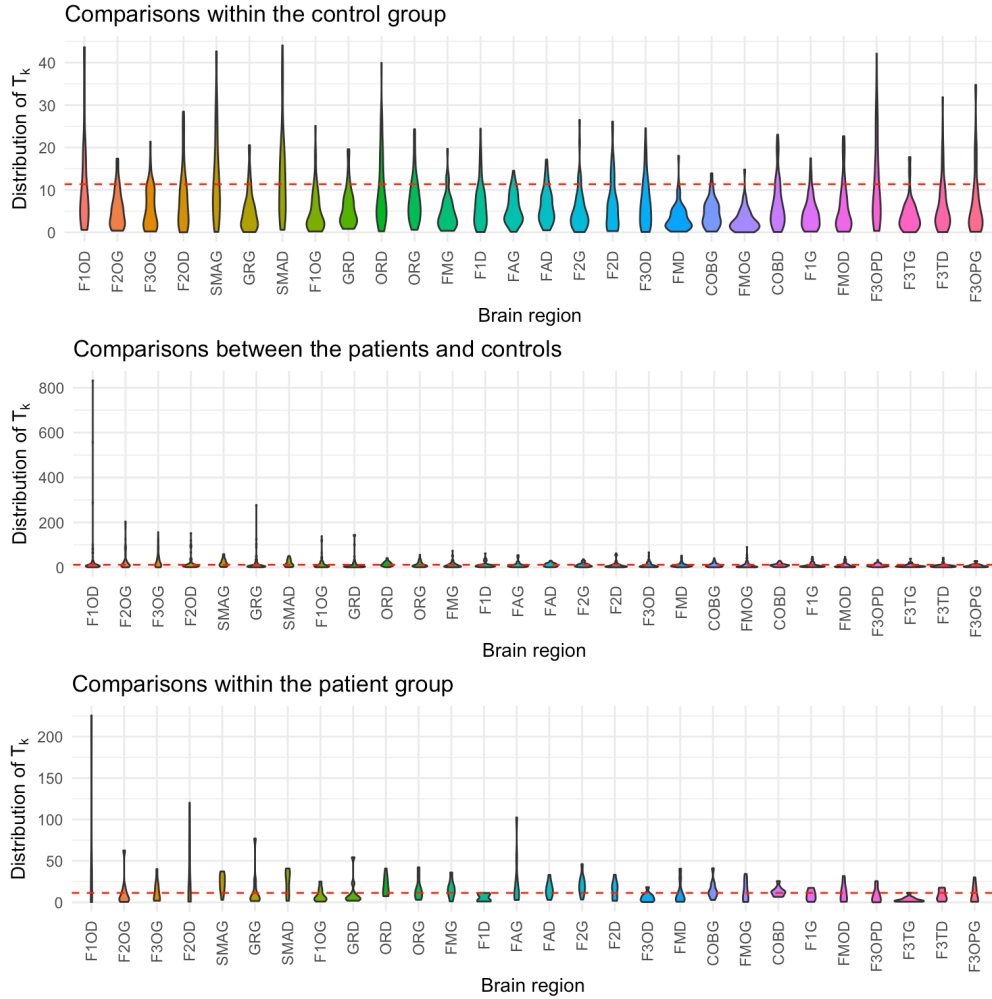


Figure A.3: Analysis of brain region latent position shifts (1) within controls, (2) between ADHD patients and controls, and (3) within patients, using Algorithm 2. The violin plots illustrate the distributions of the test statistic T_k for these three scenarios. The horizontal red dashed lines represent the critical value for detecting shifts, as specified in Theorem 3.

B Proofs of Main Results

B.1 Proof of Theorem 1

We first state two important technical lemmas, one for the error of $\hat{\mathbf{X}}^{(i)}$ as an estimate for the true $\mathbf{X}^{(i)}$ for each $i = 1, 2$, and another for the difference between $\mathbf{W}^{(1)\top} \hat{\mathbf{W}}^{(1,2)} \mathbf{W}^{(2)}$ and $\mathbf{W}^{(1,2)}$.

Lemma B.1. *Consider the setting in Theorem 1. Define $\mathbf{W}^{(i)}$ as a minimizer of $\|\hat{\mathbf{U}}^{(i)} \mathbf{O} - \mathbf{U}^{(i)}\|_F$ over all $d \times d$ orthogonal matrix \mathbf{O} . We then have*

$$\hat{\mathbf{X}}^{(i)} \mathbf{W}^{(i)} - \mathbf{X}^{(i)} = \mathbf{E}^{(i)} \mathbf{X}^{(i)} (\mathbf{X}^{(i)\top} \mathbf{X}^{(i)})^{-1} + \mathbf{R}^{(i)}, \quad (\text{B.1})$$

where $\mathbf{R}^{(i)}$ is a $n \times d$ matrix satisfying

$$\|\mathbf{R}^{(i)}\|_{2 \rightarrow \infty} \lesssim n^{-1/2} (n\rho_n)^{-1/2} \log n$$

with high probability, and thus

$$\|\hat{\mathbf{X}}^{(i)} \mathbf{W}^{(i)} - \mathbf{X}^{(i)}\|_{2 \rightarrow \infty} \lesssim n^{-1/2} \log^{1/2} n$$

with high probability.

Lemma B.1 is an application of Theorem 3.2 of Xie [2024].

Lemma B.2. *Consider the setting in Theorem 1. We then have*

$$\|\mathbf{W}^{(1)\top} \hat{\mathbf{W}}^{(1,2)} \mathbf{W}^{(2)} - \mathbf{W}^{(1,2)}\| \lesssim |\mathcal{S}|^{-1/2} (n\rho_n)^{-1/2} \log^{1/2} n + (n\rho_n)^{-1} \log n$$

with high probability.

The proof of Lemma B.2 is presented in Section C.1.

We now proceed with the proof of Theorem 1. Let $\xi_i := \hat{\mathbf{X}}^{(i)} \mathbf{W}^{(i)} - \mathbf{X}^{(i)}$ for $i = 1, 2$.

We decompose $\hat{\mathbf{Y}}\mathbf{W}^{(2)}$ as

$$\begin{aligned}
\hat{\mathbf{Y}}\mathbf{W}^{(2)} &= (\hat{\mathbf{X}}^{(2)} - \hat{\mathbf{X}}^{(1)}\hat{\mathbf{W}}^{(1,2)})\mathbf{W}^{(2)} \\
&= \xi_2 + \mathbf{X}^{(2)} - (\xi_1 + \mathbf{X}^{(1)})\mathbf{W}^{(1)\top}\hat{\mathbf{W}}^{(1,2)}\mathbf{W}^{(2)} \\
&= \xi_2 + (\mathbf{X}^{(1)}\mathbf{W}^{(1,2)} + \mathbf{Y}) - (\xi_1 + \mathbf{X}^{(1)})\mathbf{W}^{(1,2)} - (\xi_1 + \mathbf{X}^{(1)})(\mathbf{W}^{(1)\top}\hat{\mathbf{W}}^{(1,2)}\mathbf{W}^{(2)} - \mathbf{W}^{(1,2)}) \\
&\quad (\text{recall Eq. (1)}) \\
&= \mathbf{Y} + \xi_2 - \xi_1\mathbf{W}^{(1,2)} - (\xi_1 + \mathbf{X}^{(1)})(\mathbf{W}^{(1)\top}\hat{\mathbf{W}}^{(1,2)}\mathbf{W}^{(2)} - \mathbf{W}^{(1,2)}) \\
&= \mathbf{Y} + (\mathbf{E}^{(2)}\mathbf{X}^{(2)}(\mathbf{X}^{(2)\top}\mathbf{X}^{(2)})^{-1} + \mathbf{R}^{(2)}) - (\mathbf{E}^{(1)}\mathbf{X}^{(1)}(\mathbf{X}^{(1)\top}\mathbf{X}^{(1)})^{-1} + \mathbf{R}^{(1)})\mathbf{W}^{(1,2)} \\
&\quad - (\xi_1 + \mathbf{X}^{(1)})(\mathbf{W}^{(1)\top}\hat{\mathbf{W}}^{(1,2)}\mathbf{W}^{(2)} - \mathbf{W}^{(1,2)}) \quad (\text{recall Eq. (B.1) in Lemma B.1}) \\
&= \mathbf{Y} + \mathbf{E}^{(2)}\mathbf{X}^{(2)}(\mathbf{X}^{(2)\top}\mathbf{X}^{(2)})^{-1} - \mathbf{E}^{(1)}\mathbf{X}^{(1)}(\mathbf{X}^{(1)\top}\mathbf{X}^{(1)})^{-1}\mathbf{W}^{(1,2)} + \mathbf{R},
\end{aligned}$$

where

$$\mathbf{R} := \mathbf{R}^{(2)} - \mathbf{R}^{(1)}\mathbf{W}^{(1,2)} - (\xi_1 + \mathbf{X}^{(1)})(\mathbf{W}^{(1)\top}\hat{\mathbf{W}}^{(1,2)}\mathbf{W}^{(2)} - \mathbf{W}^{(1,2)}).$$

Note

$$\|\mathbf{X}^{(i)}\|_{2 \rightarrow \infty} \leq \|\mathbf{U}^{(1)}\|_{2 \rightarrow \infty} \cdot \|(\boldsymbol{\Lambda}^{(1)})^{1/2}\| \lesssim n^{-1/2}(n\rho_n)^{1/2},$$

and by Lemma B.1, Lemma B.2 we have

$$\begin{aligned}
\|\mathbf{R}\|_{2 \rightarrow \infty} &\lesssim \|\mathbf{R}^{(2)}\|_{2 \rightarrow \infty} + \|\mathbf{R}^{(1)}\|_{2 \rightarrow \infty} + (\|\xi_1\|_{2 \rightarrow \infty} + \|\mathbf{X}^{(i)}\|_{2 \rightarrow \infty}) \cdot \|\mathbf{W}^{(1)\top}\hat{\mathbf{W}}^{(1,2)}\mathbf{W}^{(2)} - \mathbf{W}^{(1,2)}\| \\
&\lesssim n^{-1/2}(n\rho_n)^{-1/2} \log n \\
&\quad + (n^{-1/2} \log^{1/2} n + n^{-1/2}(n\rho_n)^{1/2}) \cdot (|\mathcal{S}|^{-1/2}(n\rho_n)^{-1/2} \log^{1/2} n + (n\rho_n)^{-1} \log n) \\
&\lesssim n^{-1/2}(n\rho_n)^{-1/2} \log n + |\mathcal{S}|^{-1/2} n^{-1/2} \log^{1/2} n + n^{-1/2}(n\rho_n)^{-1/2} \log n \\
&\lesssim |\mathcal{S}|^{-1/2} n^{-1/2} \log^{1/2} n + n^{-1/2}(n\rho_n)^{-1/2} \log n
\end{aligned}$$

with high probability. □

B.2 Proof of Theorem 2

From Theorem 1, for the k th rows $\hat{\mathbf{y}}_k$ of $\hat{\mathbf{Y}}$ and \mathbf{y}_k of \mathbf{Y} , let

$$\boldsymbol{\theta}^{(k)} := (\mathbf{X}^{(2)\top}\mathbf{X}^{(2)})^{-1}\mathbf{X}^{(2)\top}\mathbf{e}_k^{(2)} - \mathbf{W}^{(1,2)\top}(\mathbf{X}^{(1)\top}\mathbf{X}^{(1)})^{-1}\mathbf{X}^{(1)\top}\mathbf{e}_k^{(1)},$$

we then have

$$\mathbf{W}^\top \hat{\mathbf{y}}_k - \mathbf{y}_k = \boldsymbol{\theta}^{(k)} + \mathbf{r}_k, \quad (\text{B.2})$$

where $\mathbf{e}_k^{(2)}, \mathbf{e}_k^{(1)}, \mathbf{r}_k$ are the k th rows of $\mathbf{E}^{(2)}, \mathbf{E}^{(1)}, \mathbf{R}$, respectively. Because $\text{Var}[\mathbf{E}_{st}^{(i)}] = \mathbf{P}_{st}^{(i)}(1 - \mathbf{P}_{st}^{(i)})$ and note that $\mathbf{E}^{(1)}$ and $\mathbf{E}^{(2)}$ are independent, we have

$$\text{Var}[\boldsymbol{\theta}^{(k)}] = \boldsymbol{\Gamma}^{(k)}.$$

Denote $\mathbf{Z}^{(2)} := (\mathbf{X}^{(2)\top} \mathbf{X}^{(2)})^{-1} \mathbf{X}^{(2)\top}$, $\mathbf{Z}^{(1)} := \mathbf{W}^{(1,2)\top} (\mathbf{X}^{(1)\top} \mathbf{X}^{(1)})^{-1} \mathbf{X}^{(1)\top}$ and let $\mathbf{z}_\ell^{(i)}$ be the ℓ th column of $\mathbf{Z}^{(i)}$ for any $\ell \in [n]$. Furthermore, let

$$\mathbf{Y}_\ell^{(k,i)} := \mathbf{E}_{k,\ell}^{(i)} \mathbf{z}_\ell^{(i)} \text{ for } i = 1, 2 \text{ and any } \ell \in [n].$$

We then have

$$\boldsymbol{\theta}^{(k)} = \sum_{i=1,2} \sum_{\ell \in [n]} \mathbf{Y}_\ell^{(k,i)}.$$

Note $\{\mathbf{Y}_\ell^{(k,1)}, \mathbf{Y}_\ell^{(k,2)}\}_{\ell \in [n]}$ are mutually independent zero-mean random vectors. Let

$$\tilde{\mathbf{Y}}_\ell^{(k,i)} := (\boldsymbol{\Gamma}^{(k)})^{-1/2} \mathbf{Y}_\ell^{(k,i)} \text{ for } i = 1, 2 \text{ and any } \ell \in [n].$$

For any fixed k and ℓ , we can bound the spectral norm of $\tilde{\mathbf{Y}}_\ell^{(k,1)}$ by

$$\begin{aligned} \|\tilde{\mathbf{Y}}_\ell^{(k,1)}\| &= \|(\boldsymbol{\Gamma}^{(k)})^{-1/2}\| \cdot \|\mathbf{E}_{k,\ell}^{(1)}\| \cdot \|\mathbf{W}^{(1,2)}\| \cdot \|(\mathbf{X}^{(1)\top} \mathbf{X}^{(1)})^{-1}\| \cdot \|\mathbf{X}^{(1)}\|_{2 \rightarrow \infty} \\ &\lesssim n^{1/2} \cdot 1 \cdot 1 \cdot (n\rho_n)^{-1} \cdot n^{-1/2} (n\rho_n)^{1/2} \lesssim (n\rho_n)^{-1/2} \end{aligned} \quad (\text{B.3})$$

almost surely. For any fixed $\epsilon > 0$, Eq. (B.3) implies that, for sufficiently large n , we have

$\|\tilde{\mathbf{Y}}_\ell^{(k,1)}\| \leq \epsilon$ almost surely; by similar analysis we also have $\|\tilde{\mathbf{Y}}_\ell^{(k,2)}\| \leq \epsilon$ almost surely.

And thus

$$\lim_{n \rightarrow \infty} \sum_{i=1,2} \sum_{\ell \in [n]} \mathbb{E}[\|\tilde{\mathbf{Y}}_\ell^{(k,i)}\|^2 \cdot \mathbb{I}\{\|\tilde{\mathbf{Y}}_\ell^{(k,i)}\| > \epsilon\}] = 0.$$

As $\epsilon > 0$ is fixed but arbitrary, the collection $\{\tilde{\mathbf{Y}}_\ell^{(k,i)}\}$ satisfies the condition of the Lindeberg-Feller central limit theorem (see e.g., Proposition 2.27 in [Van der Vaart \[2000\]](#)) and hence

$$(\boldsymbol{\Gamma}^{(k)})^{-1/2} \boldsymbol{\theta}^{(k)} \rightsquigarrow \mathcal{N}(\mathbf{0}, \mathbf{I}) \quad (\text{B.4})$$

as $n \rightarrow \infty$. By Theorem 1, we also have

$$\begin{aligned} \|(\mathbf{\Gamma}^{(k)})^{-1/2} \mathbf{r}_k\| &\lesssim \|(\mathbf{\Gamma}^{(k)})^{-1/2}\| \cdot \|\mathbf{R}\|_{2 \rightarrow \infty} \\ &\lesssim n^{1/2} \cdot (|\mathcal{S}|^{-1/2} n^{-1/2} \log^{1/2} n + n^{-1/2} (n\rho_n)^{-1/2} \log n) \\ &\lesssim |\mathcal{S}|^{-1/2} \log^{1/2} n + (n\rho_n)^{-1/2} \log n \end{aligned}$$

with high probability. Thus we have

$$(\mathbf{\Gamma}^{(k)})^{-1/2} \mathbf{r}_k \xrightarrow{p} \mathbf{0} \quad (\text{B.5})$$

as $n \rightarrow \infty$ provided that $|\mathcal{S}| = \omega(\log n)$ and $n\rho_n = \omega(\log^2 n)$. Combining Eq. (B.2), Eq. (B.4), Eq. (B.5), and applying Slutsky's theorem, the desired result is obtained. \square

B.3 Proof of Theorem 3

Define

$$\zeta_k := \hat{\mathbf{y}}_k^\top \mathbf{W} (\mathbf{\Gamma}^{(k)})^{-1} \mathbf{W}^\top \hat{\mathbf{y}}_k.$$

Under \mathbb{H}_0 we have $\zeta_k \rightsquigarrow \chi_d^2$; see Eq. (2). As d is finite, we conclude that ζ_k is bounded in probability. By the assumption $\lambda_\ell(\mathbf{\Gamma}^{(k)}) \asymp n^{-1}$ for all $\ell \in [d]$, we have $\lambda_\ell((\mathbf{\Gamma}^{(k)})^{-1}) \asymp n$ for all $\ell \in [d]$. We thus have $\zeta_k \asymp n \|\hat{\mathbf{y}}_k\|_F^2$, i.e., $n \|\hat{\mathbf{y}}_k\|_F^2$ is bounded in probability. Now recall the definition of T_k in Theorem 3. We then by Lemma 1 have

$$\begin{aligned} |T_k - \zeta_k| &\leq \|\mathbf{W} (\mathbf{\Gamma}^{(k)})^{-1} \mathbf{W}^\top - (\hat{\mathbf{\Gamma}}^{(k)})^{-1}\| \cdot \|\hat{\mathbf{y}}_k\|_F^2 \\ &\lesssim [(n\rho_n)^{-1/2} \log^{1/2} n] \cdot [n \|\hat{\mathbf{y}}_k\|_F^2] \xrightarrow{p} 0 \end{aligned} \quad (\text{B.6})$$

provided that $n\rho_n = \omega(\log n)$. Therefore, by Slutsky's theorem we have $T_k \rightsquigarrow \chi_d^2$ under \mathbb{H}_0 .

We now consider the case where $\mathbf{y}_k \neq \mathbf{0}$ satisfies a local alternative hypothesis where

$$\mathbf{y}_k^\top (\mathbf{\Gamma}^{(k)})^{-1} \mathbf{y}_k \rightarrow \eta \quad (\text{B.7})$$

for some finite $\eta > 0$. Define $\xi_k = (\mathbf{\Gamma}^{(k)})^{-1/2} \mathbf{y}_k$, and then Eq. (B.7) means $\|\xi_k\|^2 \rightarrow \eta$.

Recall Theorem 2. In particular we have

$$(\mathbf{\Gamma}^{(k)})^{-1/2} \mathbf{W}^\top \hat{\mathbf{y}}_k - \xi_k \rightsquigarrow \mathcal{N}(\mathbf{0}, \mathbf{I}).$$

We therefore have $\zeta_k \rightsquigarrow \chi_d^2(\eta)$, where ζ_k is defined at the beginning of the current proof. As η is finite, we conclude that ζ_k is bounded in probability. Finally, using the same argument as that for deriving Eq. (B.6) under \mathbb{H}_0 , we also have $|T_k - \zeta_k| \xrightarrow{p} 0$ under the local alternative in Eq. (B.7) and hence $T_k \rightsquigarrow \chi_d^2(\eta)$ as desired. \square

C Technical lemmas

Lemma C.3. *Consider the setting in Theorem 1. Then for $i, j \in \{1, 2\}$ we have*

$$\begin{aligned} \|\mathbf{E}^{(i)}\| &\lesssim (n\rho_n)^{1/2}, & \|\mathbf{U}^{(i)\top} \mathbf{E}^{(i)} \mathbf{U}^{(i)}\| &\lesssim (\rho_n \log n)^{1/2}, \\ \|\mathbf{E}^{(i)} \mathbf{U}^{(i)}\|_{2 \rightarrow \infty} &\lesssim (\rho_n \log n)^{1/2} \end{aligned}$$

with high probability, and

$$\|\mathbf{U}_{\mathcal{S}}^{(i)\top} \mathbf{E}_{\mathcal{S}}^{(j)} \mathbf{U}^{(j)}\| \lesssim (\rho_n \log n)^{1/2} \cdot |\mathcal{S}|^{1/2} n^{-1/2}$$

with high probability.

Lemma C.3 is derived using the same arguments as Lemma 2 in Zheng and Tang [2022]. While Lemma 2 in Zheng and Tang [2022] is stated for asymmetric matrices, a little extra care is required in the proof of Lemma C.3, as the dependency among the entries of $\mathbf{E}^{(j)}$ leads to slightly more involved book-keeping.

Lemma C.4. *Consider the setting in Theorem 1. Then for $i, j \in \{1, 2\}$ we have*

$$\begin{aligned} \lambda_k(\mathbf{A}^{(i)}) &\asymp n\rho_n \text{ for } k = 1, \dots, d, \\ \lambda_k(\mathbf{A}^{(i)}) &\lesssim (n\rho_n)^{1/2} \text{ for } k = d + 1, \dots, n \end{aligned}$$

with high probability.

Using Lemma C.3 and Weyl's inequality, we obtain the desired results for the eigenvalues of $\mathbf{A}^{(i)}$.

Lemma C.5. *Consider the setting in Theorem 1. Then for $i, j \in \{1, 2\}$ we have*

$$\begin{aligned}\|\hat{\mathbf{U}}^{(i)} \mathbf{W}^{(i)} - \mathbf{U}^{(i)}\| &\lesssim (n\rho_n)^{-1/2}, \\ \|\mathbf{W}^{(i)} (\boldsymbol{\Lambda}^{(i)})^{-1/2} - (\hat{\boldsymbol{\Lambda}}^{(i)})^{-1/2} \mathbf{W}^{(i)}\| &\lesssim n^{-1/2} (n\rho_n)^{-1} \log^{1/2} n\end{aligned}$$

with high probability.

Using Lemmas C.3 and C.4, and following the proof of Lemma B.3 in Xie [2024], we derive the results for Lemma C.5.

C.1 Proof of Lemma B.2

Note that

$$\begin{aligned}\mathbf{W}^{(1)\top} \hat{\mathbf{W}}^{(1,2)} \mathbf{W}^{(2)} &= \arg \min_{\mathbf{O} \in \mathcal{O}_d} \|\hat{\mathbf{X}}_S^{(1)} \mathbf{W}^{(1)} \mathbf{O} - \hat{\mathbf{X}}_S^{(2)} \mathbf{W}^{(2)}\|_F, \\ \mathbf{W}^{(1,2)} &= \arg \min_{\mathbf{O} \in \mathcal{O}_d} \|\mathbf{X}_S^{(1)} \mathbf{O} - \mathbf{X}_S^{(2)}\|_F.\end{aligned}$$

Denote

$$\mathbf{F} := \mathbf{W}^{(1)\top} \hat{\mathbf{X}}_S^{(1)\top} \hat{\mathbf{X}}_S^{(2)} \mathbf{W}^{(2)} - \mathbf{X}_S^{(1)\top} \mathbf{X}_S^{(2)}.$$

We therefore have, by perturbation bounds for polar decompositions, that

$$\|\mathbf{W}^{(1)\top} \hat{\mathbf{W}}^{(1,2)} \mathbf{W}^{(2)} - \mathbf{W}^{(1,2)}\| \leq \frac{2\|\mathbf{F}\|}{\sigma_{\min}(\mathbf{X}_S^{(1)\top} \mathbf{X}_S^{(2)})}. \quad (\text{C.8})$$

Indeed, from Assumption 1, $\mathbf{X}_S^{(1)\top} \mathbf{X}_S^{(2)}$ is invertible. Now suppose $\|\mathbf{F}\| < \sigma_{\min}(\mathbf{X}_S^{(1)\top} \mathbf{X}_S^{(2)})$.

Then $\hat{\mathbf{X}}_S^{(1)\top} \hat{\mathbf{X}}_S^{(2)}$ is also invertible and hence, by Theorem 1 in Li [1995] we have

$$\|\mathbf{W}^{(1)\top} \hat{\mathbf{W}}^{(1,2)} \mathbf{W}^{(2)} - \mathbf{W}^{(1,2)}\| \leq \frac{2\|\mathbf{F}\|}{\sigma_{\min}(\hat{\mathbf{X}}_S^{(1)\top} \hat{\mathbf{X}}_S^{(2)}) + \sigma_{\min}(\mathbf{X}_S^{(1)\top} \mathbf{X}_S^{(2)})} \leq \frac{2\|\mathbf{F}\|}{\sigma_{\min}(\mathbf{X}_S^{(1)\top} \mathbf{X}_S^{(2)})}.$$

Otherwise if $\|\mathbf{F}\| \geq \sigma_{\min}(\mathbf{X}_S^{(1)\top} \mathbf{X}_S^{(2)})$ then, as $\|\mathbf{W}^{(1)\top} \hat{\mathbf{W}}^{(1,2)} \mathbf{W}^{(2)} - \mathbf{W}^{(1,2)}\| \leq 2$, Eq. (C.8)

holds trivially.

We now bound the spectral norm of \mathbf{F} . First note that

$$\mathbf{F} = (\hat{\mathbf{X}}_S^{(1)} \mathbf{W}^{(1)} - \mathbf{X}_S^{(1)})^\top (\hat{\mathbf{X}}_S^{(2)} \mathbf{W}^{(2)} - \mathbf{X}_S^{(2)}) + (\hat{\mathbf{X}}_S^{(1)} \mathbf{W}^{(1)} - \mathbf{X}_S^{(1)})^\top \mathbf{X}_S^{(2)} + \mathbf{X}_S^{(1)\top} (\hat{\mathbf{X}}_S^{(2)} \mathbf{W}^{(2)} - \mathbf{X}_S^{(2)}).$$

Next, by Eq. (B.1) in Lemma B.1, we have

$$\hat{\mathbf{X}}_{\mathcal{S}}^{(i)} \mathbf{W}^{(i)} - \mathbf{X}_{\mathcal{S}}^{(i)} = \mathbf{E}_{\mathcal{S}}^{(i)} \mathbf{X}^{(i)} (\mathbf{X}^{(i)\top} \mathbf{X}^{(i)})^{-1} + \mathbf{R}_{\mathcal{S}}^{(i)} = \mathbf{E}_{\mathcal{S}}^{(i)} \mathbf{U}^{(i)} (\boldsymbol{\Lambda}^{(i)})^{-1/2} + \mathbf{R}_{\mathcal{S}}^{(i)},$$

where $\mathbf{E}_{\mathcal{S}}^{(i)}$ and $\mathbf{R}_{\mathcal{S}}^{(i)}$ contain the rows in $\mathbf{E}^{(i)}$ and $\mathbf{R}^{(i)}$ corresponding to \mathcal{S} , respectively; note that $\mathbf{X}_{\mathcal{S}}^{(i)} = \mathbf{U}_{\mathcal{S}}^{(i)} (\boldsymbol{\Lambda}^{(i)})^{1/2}$. We therefore have

$$\begin{aligned} \mathbf{F} &= (\hat{\mathbf{X}}_{\mathcal{S}}^{(1)} \mathbf{W}^{(1)} - \mathbf{X}_{\mathcal{S}}^{(1)})^\top (\hat{\mathbf{X}}_{\mathcal{S}}^{(2)} \mathbf{W}^{(2)} - \mathbf{X}_{\mathcal{S}}^{(2)}) \\ &\quad + (\boldsymbol{\Lambda}^{(1)})^{-1/2} \mathbf{U}^{(1)\top} \mathbf{E}_{\mathcal{S}}^{(1)\top} \mathbf{U}_{\mathcal{S}}^{(2)} (\boldsymbol{\Lambda}^{(2)})^{1/2} + (\boldsymbol{\Lambda}^{(1)})^{1/2} \mathbf{U}_{\mathcal{S}}^{(1)\top} \mathbf{E}_{\mathcal{S}}^{(2)} \mathbf{U}^{(2)} (\boldsymbol{\Lambda}^{(2)})^{-1/2} \\ &\quad + \mathbf{R}_{\mathcal{S}}^{(1)\top} \mathbf{U}_{\mathcal{S}}^{(2)} (\boldsymbol{\Lambda}^{(2)})^{1/2} + (\boldsymbol{\Lambda}^{(1)})^{1/2} \mathbf{U}_{\mathcal{S}}^{(1)\top} \mathbf{R}_{\mathcal{S}}^{(2)}. \end{aligned}$$

Note for any matrix $\mathbf{M} \in \mathbb{R}^{d_1 \times d_2}$, we have $\|\mathbf{M}\| \leq \|\mathbf{M}\|_F \leq d_1^{1/2} \|\mathbf{M}\|_{2 \rightarrow \infty}$. Then by Lemma B.1 and Lemma C.3 we have

$$\begin{aligned} \|\mathbf{F}\| &\leq |\mathcal{S}|^{1/2} \cdot \|\hat{\mathbf{X}}_{\mathcal{S}}^{(1)} \mathbf{W}^{(1)} - \mathbf{X}_{\mathcal{S}}^{(1)}\|_{2 \rightarrow \infty} \cdot |\mathcal{S}|^{1/2} \cdot \|\hat{\mathbf{X}}_{\mathcal{S}}^{(2)} \mathbf{W}^{(2)} - \mathbf{X}_{\mathcal{S}}^{(2)}\|_{2 \rightarrow \infty} \\ &\quad + \|(\boldsymbol{\Lambda}^{(1)})^{-1/2}\| \cdot \|\mathbf{U}^{(1)\top} \mathbf{E}_{\mathcal{S}}^{(1)\top} \mathbf{U}_{\mathcal{S}}^{(2)}\| \cdot \|(\boldsymbol{\Lambda}^{(2)})^{1/2}\| + \|(\boldsymbol{\Lambda}^{(1)})^{1/2}\| \cdot \|\mathbf{U}_{\mathcal{S}}^{(1)\top} \mathbf{E}_{\mathcal{S}}^{(2)} \mathbf{U}^{(2)}\| \cdot \|(\boldsymbol{\Lambda}^{(2)})^{-1/2}\| \\ &\quad + |\mathcal{S}|^{1/2} \|\mathbf{R}_{\mathcal{S}}^{(1)}\|_{2 \rightarrow \infty} \cdot |\mathcal{S}|^{1/2} \|\mathbf{U}_{\mathcal{S}}^{(2)}\|_{2 \rightarrow \infty} \cdot \|(\boldsymbol{\Lambda}^{(2)})^{1/2}\| + \|(\boldsymbol{\Lambda}^{(1)})^{1/2}\| \cdot |\mathcal{S}|^{1/2} \|\mathbf{U}_{\mathcal{S}}^{(1)}\|_{2 \rightarrow \infty} \cdot |\mathcal{S}|^{1/2} \|\mathbf{R}_{\mathcal{S}}^{(2)}\|_{2 \rightarrow \infty} \\ &\lesssim |\mathcal{S}|^{1/2} \cdot n^{-1/2} \log^{1/2} n \cdot |\mathcal{S}|^{1/2} \cdot n^{-1/2} \log^{1/2} n + (n\rho_n)^{-1/2} \cdot ((\rho_n \log n)^{1/2} \cdot |\mathcal{S}|^{1/2} n^{-1/2}) \cdot (n\rho_n)^{1/2} \\ &\quad + (|\mathcal{S}|^{1/2} \cdot n^{-1/2} (n\rho_n)^{-1/2} \log n) \cdot (|\mathcal{S}|^{1/2} \cdot n^{-1/2}) \cdot (n\rho_n)^{1/2} \\ &\lesssim |\mathcal{S}| n^{-1} \log n + |\mathcal{S}|^{1/2} n^{-1/2} (\rho_n \log n)^{1/2} + |\mathcal{S}| n^{-1} \log n \\ &\lesssim |\mathcal{S}|^{1/2} n^{-1} (n\rho_n)^{1/2} \log^{1/2} n + |\mathcal{S}| n^{-1} \log n \end{aligned}$$

with high probability. Note $\sigma_d(\mathbf{X}_{\mathcal{S}}^{(1)\top} \mathbf{X}_{\mathcal{S}}^{(2)}) = \sigma_d(\mathbf{X}_{\mathcal{S}}^{(1)\top} \mathbf{X}_{\mathcal{S}}^{(1)}) = (\sigma_d(\mathbf{X}_{\mathcal{S}}^{(1)}))^2 \gtrsim \frac{|\mathcal{S}|}{n} \lambda_d(\mathbf{P}^{(1)}) \asymp |\mathcal{S}| \rho_n$. Finally by Eq. (C.8) we obtain

$$\begin{aligned} \|\mathbf{W}^{(1)\top} \hat{\mathbf{W}}^{(1,2)} \mathbf{W}^{(2)} - \mathbf{W}^{(1,2)}\| &\lesssim \frac{\|\mathbf{F}\|}{\sigma_d(\mathbf{X}_{\mathcal{S}}^{(1)\top} \mathbf{X}_{\mathcal{S}}^{(2)})} \lesssim \frac{|\mathcal{S}|^{1/2} n^{-1} (n\rho_n)^{1/2} \log^{1/2} n + |\mathcal{S}| n^{-1} \log n}{|\mathcal{S}| \rho_n} \\ &\lesssim |\mathcal{S}|^{-1/2} (n\rho_n)^{-1/2} \log^{1/2} n + (n\rho_n)^{-1} \log n \end{aligned}$$

with high probability. \square

C.2 Proof of Lemma 1

We first derive an upper bound of $\|\mathbf{W}\Gamma^{(k)}\mathbf{W}^\top - \hat{\Gamma}^{(k)}\|$. Let

$$\begin{aligned}\mathbf{H}_1 &:= \mathbf{W}^{(2)}(\mathbf{X}^{(2)\top}\mathbf{X}^{(2)})^{-1}\mathbf{X}^{(2)\top}\boldsymbol{\Xi}^{(k,2)}\mathbf{X}^{(2)}(\mathbf{X}^{(2)\top}\mathbf{X}^{(2)})^{-1}\mathbf{W}^{(2)\top} - (\hat{\mathbf{X}}^{(2)\top}\hat{\mathbf{X}}^{(2)})^{-1}\hat{\mathbf{X}}^{(2)\top}\hat{\boldsymbol{\Xi}}^{(k,2)}\hat{\mathbf{X}}^{(2)}(\hat{\mathbf{X}}^{(2)\top}\hat{\mathbf{X}}^{(2)})^{-1} \\ \mathbf{H}_2 &:= \mathbf{W}^{(2)}\mathbf{W}^{(1,2)\top}(\mathbf{X}^{(1)\top}\mathbf{X}^{(1)})^{-1}\mathbf{X}^{(1)\top}\boldsymbol{\Xi}^{(k,1)}\mathbf{X}^{(1)}(\mathbf{X}^{(1)\top}\mathbf{X}^{(1)})^{-1}\mathbf{W}^{(1,2)}\mathbf{W}^{(2)\top} \\ &\quad - \hat{\mathbf{W}}^{(1,2)\top}(\hat{\mathbf{X}}^{(1)\top}\hat{\mathbf{X}}^{(1)})^{-1}\hat{\mathbf{X}}^{(1)\top}\hat{\boldsymbol{\Xi}}^{(k,1)}\hat{\mathbf{X}}^{(1)}(\hat{\mathbf{X}}^{(1)\top}\hat{\mathbf{X}}^{(1)})^{-1}\hat{\mathbf{W}}^{(1,2)}.\end{aligned}$$

Then $\mathbf{W}\Gamma^{(k)}\mathbf{W}^\top - \hat{\Gamma}^{(k)} = \mathbf{H}_1 + \mathbf{H}_2$. We now bound \mathbf{H}_1 and \mathbf{H}_2 , respectively. For \mathbf{H}_1 , we have

$$\begin{aligned}\|\mathbf{H}_1\| &\leq \|\mathbf{W}^{(2)}(\mathbf{X}^{(2)\top}\mathbf{X}^{(2)})^{-1}\mathbf{X}^{(2)\top} - (\hat{\mathbf{X}}^{(2)\top}\hat{\mathbf{X}}^{(2)})^{-1}\hat{\mathbf{X}}^{(2)\top}\| \cdot \|\boldsymbol{\Xi}^{(k,2)}\| \cdot \|\mathbf{X}^{(2)}(\mathbf{X}^{(2)\top}\mathbf{X}^{(2)})^{-1}\| \\ &\quad + \|(\hat{\mathbf{X}}^{(2)\top}\hat{\mathbf{X}}^{(2)})^{-1}\hat{\mathbf{X}}^{(2)\top}\| \cdot \|\boldsymbol{\Xi}^{(k,2)}\| \cdot \|\mathbf{X}^{(2)}(\mathbf{X}^{(2)\top}\mathbf{X}^{(2)})^{-1}\mathbf{W}^{(2)\top} - \hat{\mathbf{X}}^{(2)}(\hat{\mathbf{X}}^{(2)\top}\hat{\mathbf{X}}^{(2)})^{-1}\| \\ &\quad + \|(\hat{\mathbf{X}}^{(2)\top}\hat{\mathbf{X}}^{(2)})^{-1}\hat{\mathbf{X}}^{(2)\top}\| \cdot \|\boldsymbol{\Xi}^{(k,2)} - \hat{\boldsymbol{\Xi}}^{(k,2)}\| \cdot \|\hat{\mathbf{X}}^{(2)}(\hat{\mathbf{X}}^{(2)\top}\hat{\mathbf{X}}^{(2)})^{-1}\|. \tag{C.9}\end{aligned}$$

We now bound the terms in Eq. (C.13) respectively. For $\mathbf{W}^{(2)}(\mathbf{X}^{(2)\top}\mathbf{X}^{(2)})^{-1}\mathbf{X}^{(2)\top} - (\hat{\mathbf{X}}^{(2)\top}\hat{\mathbf{X}}^{(2)})^{-1}\hat{\mathbf{X}}^{(2)\top}$, we have

$$\begin{aligned}&\mathbf{W}^{(2)}(\mathbf{X}^{(2)\top}\mathbf{X}^{(2)})^{-1}\mathbf{X}^{(2)\top} - (\hat{\mathbf{X}}^{(2)\top}\hat{\mathbf{X}}^{(2)})^{-1}\hat{\mathbf{X}}^{(2)\top} \\ &= \mathbf{W}^{(2)}(\boldsymbol{\Lambda}^{(2)})^{-1/2}\mathbf{U}^{(2)\top} - (\hat{\boldsymbol{\Lambda}}^{(2)})^{-1/2}\hat{\mathbf{U}}^{(2)\top} \\ &= [\mathbf{W}^{(2)}(\boldsymbol{\Lambda}^{(2)})^{-1/2} - (\hat{\boldsymbol{\Lambda}}^{(2)})^{-1/2}\mathbf{W}^{(2)}]\mathbf{U}^{(2)\top} + (\hat{\boldsymbol{\Lambda}}^{(2)})^{-1/2}\mathbf{W}^{(2)}[\mathbf{U}^{(2)} - \hat{\mathbf{U}}^{(2)}\mathbf{W}^{(2)}]^\top.\end{aligned}$$

Then by Lemmas C.4 and C.5 we have

$$\begin{aligned}&\|\mathbf{W}^{(2)}(\mathbf{X}^{(2)\top}\mathbf{X}^{(2)})^{-1}\mathbf{X}^{(2)\top} - (\hat{\mathbf{X}}^{(2)\top}\hat{\mathbf{X}}^{(2)})^{-1}\hat{\mathbf{X}}^{(2)\top}\| \\ &\leq \|\mathbf{W}^{(2)}(\boldsymbol{\Lambda}^{(2)})^{-1/2} - (\hat{\boldsymbol{\Lambda}}^{(2)})^{-1/2}\mathbf{W}^{(2)}\| + \|(\hat{\boldsymbol{\Lambda}}^{(2)})^{-1/2}\| \cdot \|\hat{\mathbf{U}}^{(2)}\mathbf{W}^{(2)} - \mathbf{U}^{(2)}\| \\ &\lesssim n^{-1/2}(n\rho_n)^{-1} \log^{1/2} n + (n\rho_n)^{-1/2} \cdot (n\rho_n)^{-1/2} \\ &\lesssim (n\rho_n)^{-1}\end{aligned}\tag{C.10}$$

with high probability. For $\boldsymbol{\Xi}^{(k,2)} - \hat{\boldsymbol{\Xi}}^{(k,2)}$, using the same arguments as that for Eq. (C.21) in Zheng and Tang [2022] we have

$$\|\boldsymbol{\Xi}^{(k,2)} - \hat{\boldsymbol{\Xi}}^{(k,2)}\| \lesssim n^{-1}(n\rho_n)^{1/2} \log^{1/2} n \tag{C.11}$$

with high probability. We also have

$$\begin{aligned}
\|\Xi^{(k,2)}\| &\leq \|\mathbf{P}^{(2)}\|_{\max} \leq \|\mathbf{U}^{(2)}\|_{2 \rightarrow \infty}^2 \cdot \|\Lambda^{(2)}\| \lesssim n^{-1}(n\rho_n), \\
\|\mathbf{X}^{(2)}(\mathbf{X}^{(2)\top}\mathbf{X}^{(2)})^{-1}\| &\leq \|(\Lambda^{(2)})^{-1/2}\| \lesssim (n\rho_n)^{-1/2}, \\
\|(\hat{\mathbf{X}}^{(2)\top}\hat{\mathbf{X}}^{(2)})^{-1}\hat{\mathbf{X}}^{(2)\top}\| &\leq \|(\hat{\Lambda}^{(2)})^{-1/2}\| \lesssim (n\rho_n)^{-1/2}
\end{aligned} \tag{C.12}$$

with high probability by Lemma C.4. Combining Eq. (C.13), Eq. (C.14), Eq. (C.15), and Eq. (C.12) we have

$$\begin{aligned}
\|\mathbf{H}_1\| &\lesssim (n\rho_n)^{-1} \cdot n^{-1}(n\rho_n) \cdot (n\rho_n)^{-1/2} + [(n\rho_n)^{-1/2}]^2 \cdot n^{-1}(n\rho_n)^{1/2} \log^{1/2} n \\
&\lesssim n^{-1}(n\rho_n)^{-1/2} + n^{-1}(n\rho_n)^{-1/2} \log^{1/2} n \lesssim n^{-1}(n\rho_n)^{-1/2} \log^{1/2} n
\end{aligned}$$

with high probability.

For \mathbf{H}_2 , we have

$$\begin{aligned}
\mathbf{H}_2 &= \underbrace{\mathbf{W}^{(2)}(\mathbf{W}^{(1,2)\top} - \mathbf{W}^{(2)\top}\hat{\mathbf{W}}^{(1,2)\top}\mathbf{W}^{(1)})(\mathbf{X}^{(1)\top}\mathbf{X}^{(1)})^{-1}\mathbf{X}^{(1)\top}\Xi^{(k,1)}\mathbf{X}^{(1)}(\mathbf{X}^{(1)\top}\mathbf{X}^{(1)})^{-1}\mathbf{W}^{(1,2)}\mathbf{W}^{(2)\top}}_{\mathbf{H}_{2,1}} \\
&+ \underbrace{\hat{\mathbf{W}}^{(1,2)\top}\mathbf{W}^{(1)}(\mathbf{X}^{(1)\top}\mathbf{X}^{(1)})^{-1}\mathbf{X}^{(1)\top}\Xi^{(k,1)}\mathbf{X}^{(1)}(\mathbf{X}^{(1)\top}\mathbf{X}^{(1)})^{-1}(\mathbf{W}^{(1,2)} - \mathbf{W}^{(1)\top}\hat{\mathbf{W}}^{(1,2)}\mathbf{W}^{(2)})\mathbf{W}^{(2)\top}}_{\mathbf{H}_{2,2}} \\
&+ \underbrace{\hat{\mathbf{W}}^{(1,2)\top}\mathbf{W}^{(1)}(\mathbf{X}^{(1)\top}\mathbf{X}^{(1)})^{-1}\mathbf{X}^{(1)\top}\Xi^{(k,1)}\mathbf{X}^{(1)}(\mathbf{X}^{(1)\top}\mathbf{X}^{(1)})^{-1}\mathbf{W}^{(1)\top}\hat{\mathbf{W}}^{(1,2)}}_{\mathbf{H}_{2,3}} \\
&+ \underbrace{[-\hat{\mathbf{W}}^{(1,2)\top}(\hat{\mathbf{X}}^{(1)\top}\hat{\mathbf{X}}^{(1)})^{-1}\hat{\mathbf{X}}^{(1)\top}\hat{\Xi}^{(k,1)}\hat{\mathbf{X}}^{(1)}(\hat{\mathbf{X}}^{(1)\top}\hat{\mathbf{X}}^{(1)})^{-1}\hat{\mathbf{W}}^{(1,2)}]}_{\mathbf{H}_{2,4}}.
\end{aligned} \tag{C.13}$$

With the identical analysis of \mathbf{H}_1 we have

$$\|\mathbf{H}_{2,3} + \mathbf{H}_{2,4}\| \lesssim n^{-1}(n\rho_n)^{-1/2} \log^{1/2} n \tag{C.14}$$

with high probability. For $\mathbf{H}_{2,1}$ and $\mathbf{H}_{2,2}$, by Lemma B.2 and Eq. (C.12) for $i = 1$ we have

$$\begin{aligned}
\|\mathbf{H}_{2,1}\| &\leq \|\mathbf{W}^{(1)\top}\hat{\mathbf{W}}^{(1,2)}\mathbf{W}^{(2)} - \mathbf{W}^{(1,2)}\| \cdot \|\mathbf{X}^{(1)}(\mathbf{X}^{(1)\top}\mathbf{X}^{(1)})^{-1}\|^2 \cdot \|\Xi^{(k,1)}\| \\
&\lesssim [|\mathcal{S}|^{-1/2}(n\rho_n)^{-1/2} \log^{1/2} n + (n\rho_n)^{-1} \log n] \cdot (n\rho_n)^{-1} \cdot n^{-1}(n\rho_n) \\
&\lesssim |\mathcal{S}|^{-1/2} n^{-1}(n\rho_n)^{-1/2} \log^{1/2} n + n^{-1}(n\rho_n)^{-1} \log n, \\
\|\mathbf{H}_{2,2}\| &\lesssim |\mathcal{S}|^{-1/2} n^{-1}(n\rho_n)^{-1/2} \log^{1/2} n + n^{-1}(n\rho_n)^{-1} \log n
\end{aligned} \tag{C.15}$$

with high probability. Combining Eq. (C.13), Eq. (C.14), and Eq. (C.15) we have

$$\begin{aligned} \|\mathbf{H}_2\| &\lesssim |\mathcal{S}|^{-1/2} n^{-1} (n\rho_n)^{-1/2} \log^{1/2} n + n^{-1} (n\rho_n)^{-1} \log n + n^{-1} (n\rho_n)^{-1/2} \log^{1/2} n \\ &\lesssim n^{-1} (n\rho_n)^{-1/2} \log^{1/2} n \end{aligned}$$

with high probability. By the above bounds for \mathbf{H}_1 and \mathbf{H}_2 we thus have

$$\|\mathbf{W}\mathbf{\Gamma}^{(k)}\mathbf{W}^\top - \hat{\mathbf{\Gamma}}^{(k)}\| \lesssim n^{-1} (n\rho_n)^{-1/2} \log^{1/2} n \quad (\text{C.16})$$

with high probability. Recall the assumption that $\lambda_\ell(\mathbf{\Gamma}^{(k)}) \asymp n^{-1}$ for all $\ell \in [d]$ in Theorem 2. Then by Weyl's theorem and Eq. (C.16) we also have $\lambda_\ell(\hat{\mathbf{\Gamma}}^{(k)}) \asymp n^{-1}$ for all $\ell \in [d]$ whenever $n\rho_n \gg \log n$. Therefore we have

$$\|\mathbf{W}(\mathbf{\Gamma}^{(k)})^{-1}\mathbf{W}^\top\| \lesssim n, \quad \|(\hat{\mathbf{\Gamma}}^{(k)})^{-1}\| \lesssim n \quad (\text{C.17})$$

with high probability. Since $\|\mathbf{A}^{-1} - \mathbf{B}^{-1}\| \leq \|\mathbf{A}^{-1}\| \cdot \|\mathbf{A} - \mathbf{B}\| \cdot \|\mathbf{B}^{-1}\|$ for any invertible matrices \mathbf{A} and \mathbf{B} , we have by Eq. (C.16) and Eq. (C.17) that

$$\|\mathbf{W}(\mathbf{\Gamma}^{(k)})^{-1}\mathbf{W}^\top - (\hat{\mathbf{\Gamma}}^{(k)})^{-1}\| \lesssim n(n\rho_n)^{-1/2} \log^{1/2} n$$

with high probability.